Miner Deposita (2015) 50:987–1006
DOI 10.1007/s00126-015-0584-1

ARTICLE

Cretaceous–Cenozoic tectonic history of the Jiaojia Fault and gold mineralization in the Jiaodong Peninsula, China: constraints from zircon U–Pb, illite K–Ar, and apatite fission track thermochronometry

Jun Deng[1] · **Changming Wang**[1,2] · **Leon Bagas**[2] · **Emmanuel John M. Carranza**[3] · **Yongjun Lu**[2]

Received: 24 September 2014 / Accepted: 6 March 2015 / Published online: 25 March 2015

Abstract The Jiaojia Fault (JJF) in the Jiaodong area of eastern China is an important NNE-trending structure that is subsidiary to the regional Tancheng–Lujiang (Tan-Lu) Fault Zone, and hosts >1200 t of gold reserves contained in disseminated and stockwork ore, dominantly in the footwall of the fault. We present new zircon U–Pb, apatite fission track, and illite K–Ar data along the JJF and have delineated its tectonic history focusing on its formation and reactivation. Zircon U–Pb dating shows that the Shangzhuang granite is a composite body with ages between 132±1 and 127±1 Ma. Illite K–Ar ages for the fault's gouge range from 83±2 to 68±2 Ma, and the measured apatite fission track ages for ores are between 55 and 21 Ma. Previous zircon U–Pb geochronology and structural studies suggest that the JJF was originally activated in the Jurassic during 160–150 Ma as a sinistral fault. The JJF was a normal fault in the Early Cretaceous due to NW–SE orientated tension and NE–SW compression, which lasted from 135 to 120 Ma. This was followed by sinistral strike–slip faulting due to NW–SE compression and NE–SW tension during 120–110 Ma, and it changed to normal displacement at ca. 110 Ma. Our apatite fission track data analysis and thermal modeling of representative samples suggest that there was a subsequent dextral reactivation of the fault at ca. 55 Ma. Previous age data of ca. 130–110 Ma for gold mineralization along the JJF coincides with the Early Cretaceous magmatism and is coeval with the transition from normal faulting to sinistral strike–slip faulting of the JJF in Early Cretaceous, which is interpreted to be due to changing direction of the subducting Pacific Plate.

Keywords Zircon U–Pb dating · Apatite fission track · Illite K–Ar age · Tectonic implications · Jiaojia Fault · Tan-Lu Fault · Jiaodong Peninsula

Editorial handling: T. Bissig and G. Beaudoin

✉ Jun Deng
djun@cugb.edu.cn

Changming Wang
wangcm@cugb.edu.cn

[1] State Key Laboratory of Geological Processes and Mineral Resources, China University of Geosciences, No. 29, Xueyuan Road, Haidian District, 100083 Beijing, China

[2] Centre for Exploration Targeting and Australian Research Council Centre of Excellence for Core to Crust Fluid Systems (CCFS), School of Earth and Environment, University of Western Australia, Perth, WA 6009, Australia

[3] School of Earth and Environmental Sciences, James Cook University, Townsville, Queensland, Australia

Introduction

The Jiaodong Peninsula is in the southeastern margin of the North China Craton and to the east of the NNE-trending Tan-Lu Fault (Fig. 1). The dominant structures in the Jiaodong area are NNE-trending faults, which are subsidiary to the regional Tan-Lu Fault (Fig. 2; Goldfarb et al. 2001; Zhou et al. 2002; Qiu et al. 2002; Fan et al. 2003).

The Tan-Lu Fault is considered to be of key significance to the tectonic evolution of eastern China (Leech and Webb 2013). In addition, gold deposits are developed along its subsidiary NNE-trending faults (Fig. 2; Deng et al. 2003, 2006, 2015). Examples include the Sanshandao and Cangshang deposits along the Sanshandao Fault; the Jiaojia, Xincheng, and Wang'ershan deposits along the Jiaojia Fault; the Zhaoyuan and Dayingezhuang deposits along the Zhaoping Fault; and the Jinniushan and Denggezhuang deposits along the Jinniushan Fault. The NNE-trending auriferous faults have a

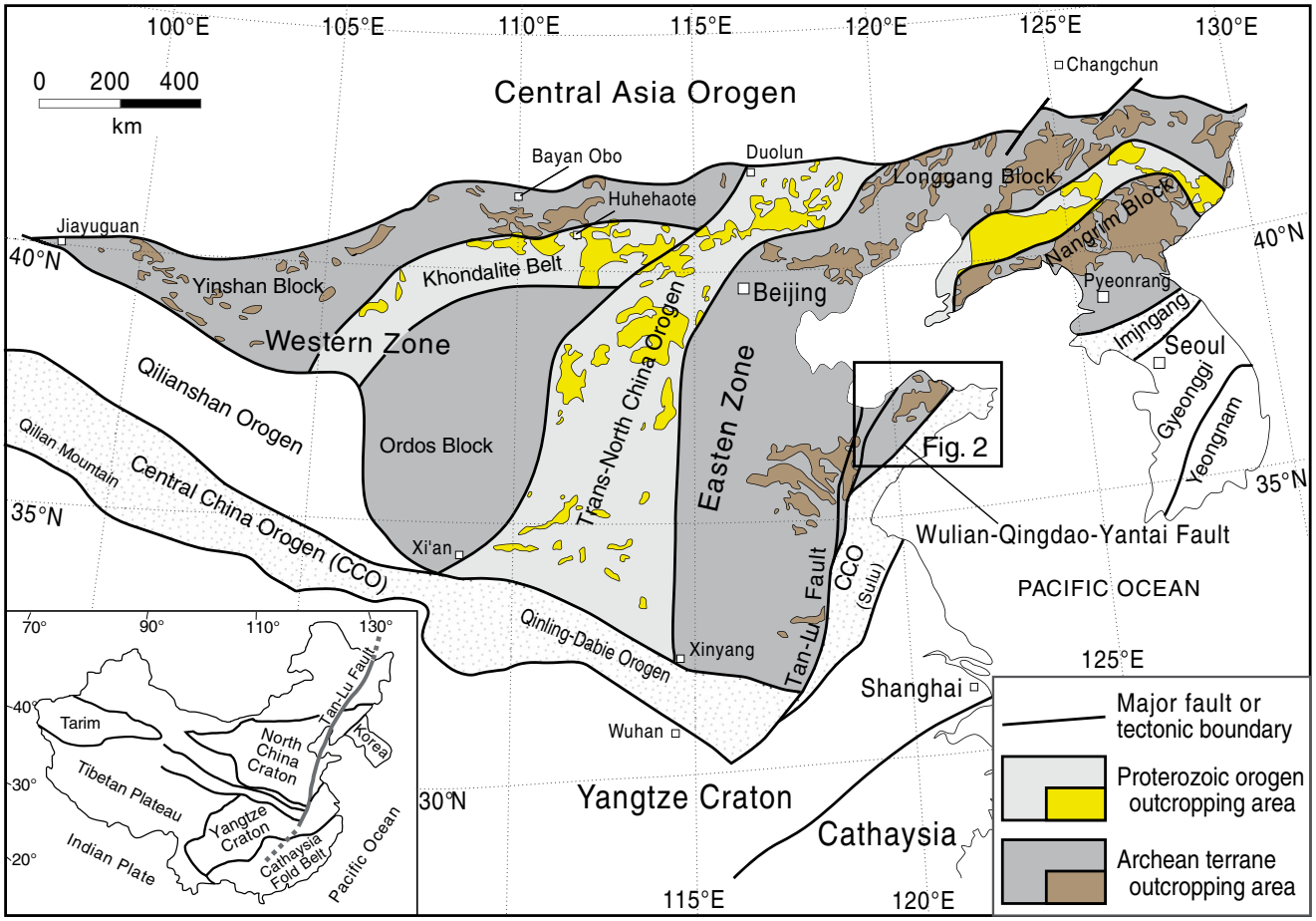

Fig. 1 Simplified geological map showing the tectonic subdivision of the North China Craton (modified from Zhao et al. 2005). *Rectangle* shows location of the study area in Fig. 2

total gold reserve of >3000 t (Goldfarb et al. 2014), of which the Jiaojia Fault (JJF) hosts a gold reserve of ~1200 t at grades of 1.01 to 26.44 g/t Au (Song et al. 2014).

Gold deposits of the Jiaodong Peninsula are divided into quartz vein-style "Linglong-type" and disseminated- and stockwork-style "Jiaojia-type" gold mineralization (Qiu et al. 2002; Deng et al. 2003; Yang et al. 2014; Wang et al. 2015). Gold deposits along the JJF are representatives of the disseminated- and stockwork-style "Jiaojia-type" of mineralization (Wang 2010). These deposits have been interpreted as orogenic deposits (Groves et al. 1998; Goldfarb et al. 2001, 2005, 2007; Kerrich et al. 2000; Qiu et al. 2002; Zhou and Lu 2000; Goldfarb et al. 2014; De Boorder 2015), magmatic–hydrothermal gold deposits (Zhai et al. 2011), or a unique class of "Jiaodong-type" gold deposits associated with intraplate tectonics (Zhai et al. 2004; Zhai and Santosh 2013; Song et al. 2014; Li et al. 2015).

Despite of the significant gold reserves hosted by the JJF, the dynamic mechanism and tectonic evolution that ultimately led to gold deposition is poorly understood, partly due to the limited data from the structure. Previous research in this area has focused on granites and gold deposits (Deng et al. 2003, 2006). However, no detailed studies have focused on the tectonic evolution of the fault and its relationship with the gold mineralization of the JJF. In this work, we present new zircon U–Pb, illite K–Ar, and apatite fission track thermochronological data along the JJF, in order to enhance our understanding of the tectonic evolution of this region and the relationship between the timing of tectonic movements of the fault and the gold mineralizations within the Jiaodong Peninsula.

Geological setting and structural characteristics

The Jiaodong Peninsula is divided by the Wulian–Qingdao–Yantai Sulu Suture into the Jiaobei Terrane in the north and the Sulu Terrane in the south (Fig. 2). The Precambrian sequences of the Jiaobei Terrane consist of the Archaean Jiaodong Group, the Paleoproterozoic Fenzishan and Jingshan Groups, and the Neoproterozoic Penglai Group (Zhou and Lu 2000). The Jiaodong Group consists of granulite, amphibolite, gneiss, and schist. The Jingshan Group consists of marble, biotite–plagioclase gneiss, and amphibolite, and the

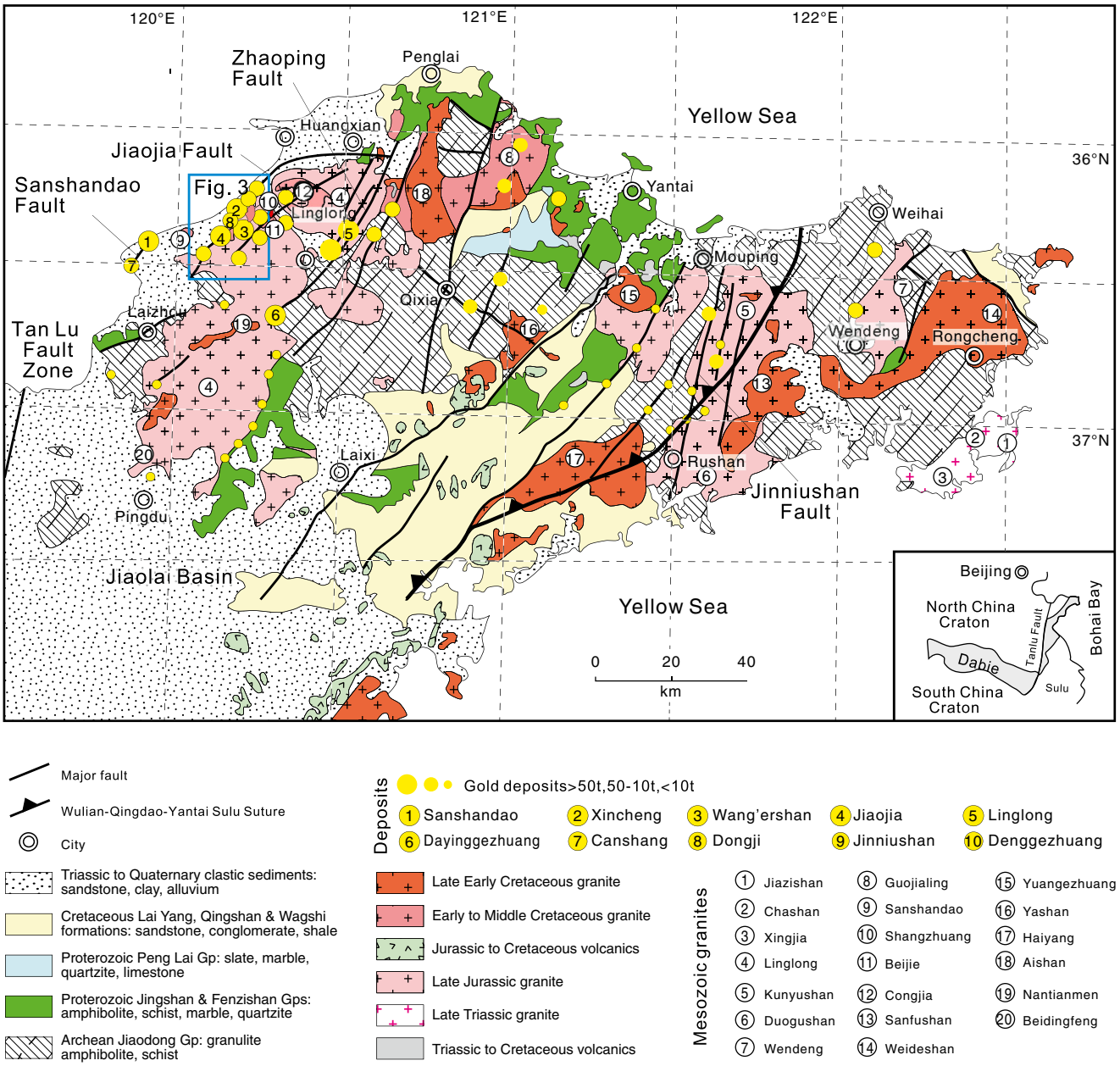

Fig. 2 Simplified geological map of the Jiaodong Peninsula showing the main tectonic units, first-order fault zones, and gold deposits (modified from Wang et al. 1998)

Fenzishan Group consists of marble, schist, gneiss, and amphibolite. The Penglai Group, which unconformably overlies both the Jingshan and Fenzishan Groups, consists of limestone, shale, and marble.

Mesozoic granitic bodies comprise >40 % of the exposed rocks in the Jiaodong Peninsula (Qiu et al. 2002) and are subdivided into (i) the Jiazishan and Chashan Triassic plutons, (ii) the Linglong and Kunyushan Jurassic plutons, and (iii) the Guojialing and the Shangzhuang Cretaceous plutons (Fig. 2). Similar Cretaceous felsic and mafic igneous rocks are present in the area of the North China Craton (NCC) with an interpreted crustal and mantle source and a transition from enriched mantle to depleted mantle (Guo et al. 2005; Liu et al. 2014). This transition has been associated with lithosphere thinning in this part of the NCC during the Mesozoic (Guo et al. 2005; Liu et al. 2014).

Regional faults within the Jiaodong Peninsula predominantly trend NNE and, to a lesser extent, to the NW. The Huangxian–Yexian arc fault zone (Huangye Fault) is one of the most important faults zones in the peninsula, and it can be divided into (1) a northern segment located in Huang County, which is characterized by ENE-trending faults dipping 30–45° to the north; and (2) a southern segment located in Ye County, which is characterized by NNE-trending faults dipping 29–

43° to the NW. The JJF is part of the southern segment of the Huangye Fault and is about 30 km long and 100–400 m wide. The JJF is characterized by a single main fault plane, marked by a gray-colored fault gouge zone that is 50–200 mm wide, which is present throughout the area. Two types of deformations with the same attitudes have affected the fault. One is ductile shear deformation, in which porphyroclasts, schistosity, augen, rotating morphology, and domino structures are well developed (Fig. 3). The other is a large-scale deformation resulting in the formation of cataclastic rocks (Wang 2010).

Jiaojia Fault and its structural controls on gold deposits

The most prominent fault in the Jiaojia mineral field is the JJF that controls the spatial distribution of gold mineralization (Fig. 3), which includes the Sizhang, Matang, Jiaojia, Wangershan, Dongji, Longbu, Hedong, Hexi, Fujia, Xincheng, and Shangzhuang deposits (Fig. 3). These deposits occur in the footwall of the JJF and the Linglong Granite as the hanging wall. Underlying the JJF include the Linglong Granite, Guojialing Granodiorite, and the Jiaodong Group.

The gold deposits along the JJF consist of disseminated- and stockwork-style mineralization. The disseminated type of mineralization extends for ~50 m below and parallel with the fault, whereas the stockwork-type mineralization extends from tens up to hundreds of meters from the fault (Fig. 4). The disseminated-type mineralization is hosted by pyritized, sericitized, and silicified granite (Fig. 5c). Alteration is characterized by sericite, quartz, and K-feldspar. The stockwork-type mineralization is hosted by potassic-altered and silicified granite (Fig. 5b, d, e).

Major minerals in the gold deposits along the JJF include native gold, electrum, native silver, iron-bearing native silver, acanthite, pyrite, sphalerite, and galena (Fig. 5f). Gangue minerals include quartz, sericite, feldspar, calcite, barite, and chlorite. The gold-bearing sulfides are pyrite, chalcopyrite, sphalerite, and galena, all of which are hosted by quartz veins.

Four mineral associations have been identified in the deposits, which are as follows: (1) quartz–K-feldspar–pyrite marking the earliest stage of mineralization; (2) quartz–pyrite–gold being the most important auriferous stage during which large amounts of pyrite, quartz, and native gold were precipitated; (3) quartz–base metal sulfides(–gold) marks a minor gold mineralization period with the precipitation of large amounts of sulfide minerals such as pyrite, galena, sphalerite, chalcopyrite, and arsenopyrite; and (4) quartz–calcite–pyrite hosted by quartz, calcite, and siderite forming veins in late fractures.

Methods and analytical procedures

Laser ablation inductively coupled plasma mass spectrometry (LA-ICP-MS) U–Pb dating

Granodiorite samples SZ-02 and XC480-03 are from the porphyritic Shangzhuang granite (Figs. 3 and 5a). The samples consist of K-feldspar (~30 vol%), plagioclase (~40 vol%), quartz (~25 vol%), biotite and amphibole (~5 vol%), and accessory titanite, apatite, zircon, and magnetite.

Zircon LA-ICP-MS U–Pb analysis was conducted at the Institute of Mineral Resources, Chinese Academy of Geological Sciences, Beijing, China. The analysis involves ablation of zircon with a NUP 213 Excimer laser using a spot diameter of 25 μm, with constant 2.5 J/cm^2 energy density, and a repetition rate of 10 Hz. Detailed operating conditions for the laser ablation system and the LA-ICP-MS instrument and the data reduction are described by Hou et al. (2009). Preferred U–Th–Pb isotopic ratios used for GJ1 are from Jackson et al. (2004). Uncertainty of preferred values for the external standard GJ1 was propagated to the ultimate results of the samples. In all analyzed zircon grains, the common Pb correction was not necessary due to the low signal of common ^{204}Pb and high ^{206}Pb/^{204}Pb. Concentrations of U, Th, and Pb were calibrated using zircon M127 (Nasdala et al. 2008). Concordia diagrams and weighted mean calculations were made using Isoplot/Ex_ver3. The zircon Plesovice is dated as unknown samples and yielded weighted mean ^{206}Pb/^{238}U age of 337±2 Ma (2σ, n=12), which is in good agreement with the recommended ^{206}Pb/^{238}U age of 337.13±0.37 Ma (2σ) (Slama et al. 2008) (Table 1).

Apatite fission track method

In order to reconstruct the thermal history of the JJF, four disseminated-style samples (SC-01, XC175-02, XC205-04, and XC480-03) and four stockwork-style samples (XC480-07, XC580-18, XC600-07, and XC600-08) of ore from the Xincheng deposit were analyzed for apatite fission track thermochronology (Table 2).

Apatite was separated by standard magnetic and heavy liquid techniques. A uranium free muscovite sheet was attached, as an external detector, to each grain mount, and neutron influence was determined using the SRM 962 uranium dosimeter glass. The apatite was etched in 6.6 % HNO_3 for 30 s at 25 °C. Etched spontaneous tracks in apatites were counted using Nikon Eclipse® E600 microscope with ×100 dry objectives and ×10 eyepieces. Fission track ages and length data were modeled following the method of Ketcham et al. (1999). Apatite composition was monitored by a combination of etch pit dimensions and absolute measurement by electron microprobe analysis using a JEOL electron microprobe, with an accelerating voltage of 15 kV, a beam current

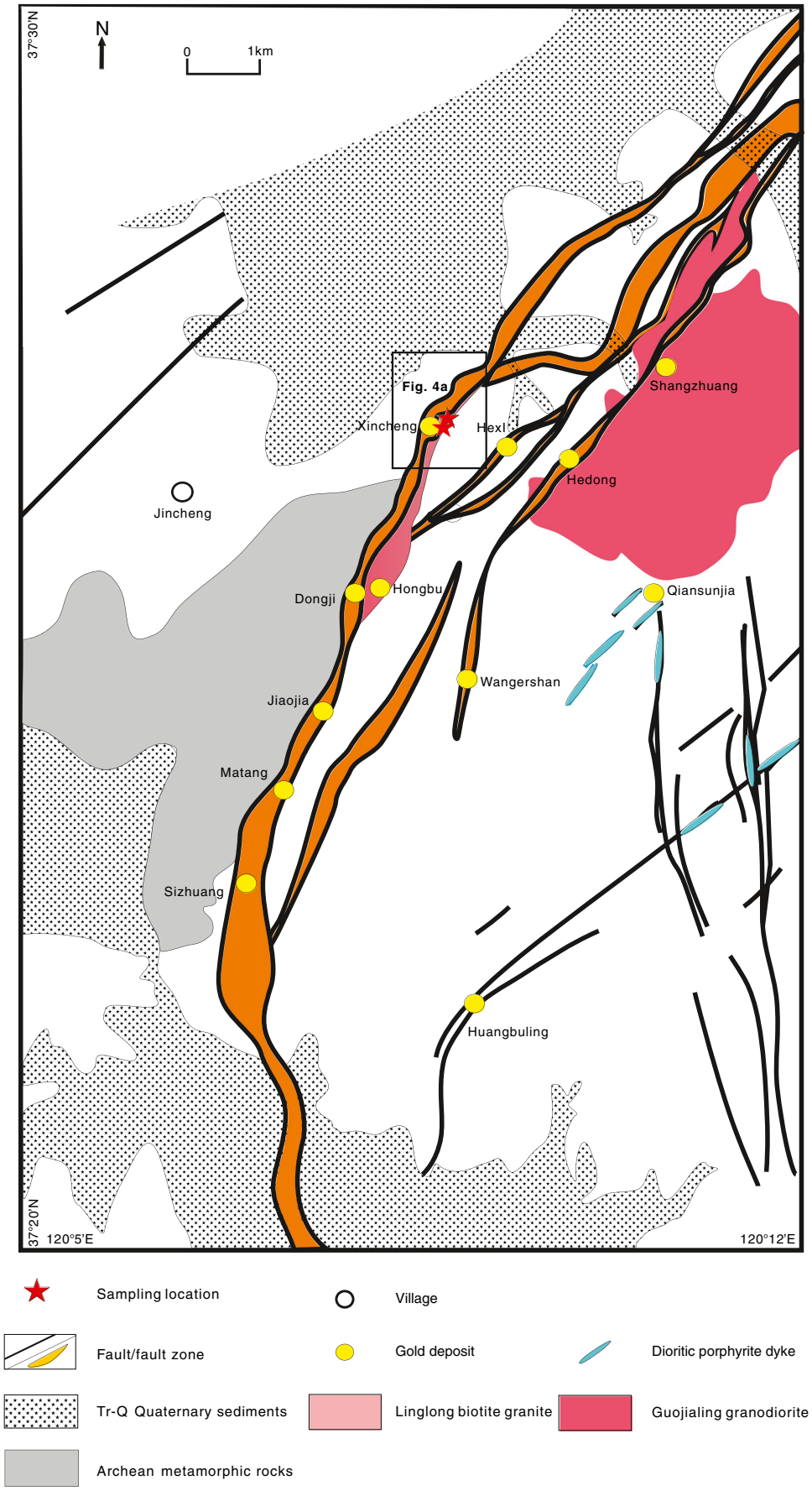

Fig. 3 The Jiaojia Fault and its structural controls on gold deposits in the Jiaojia ore field (Wang 2010)

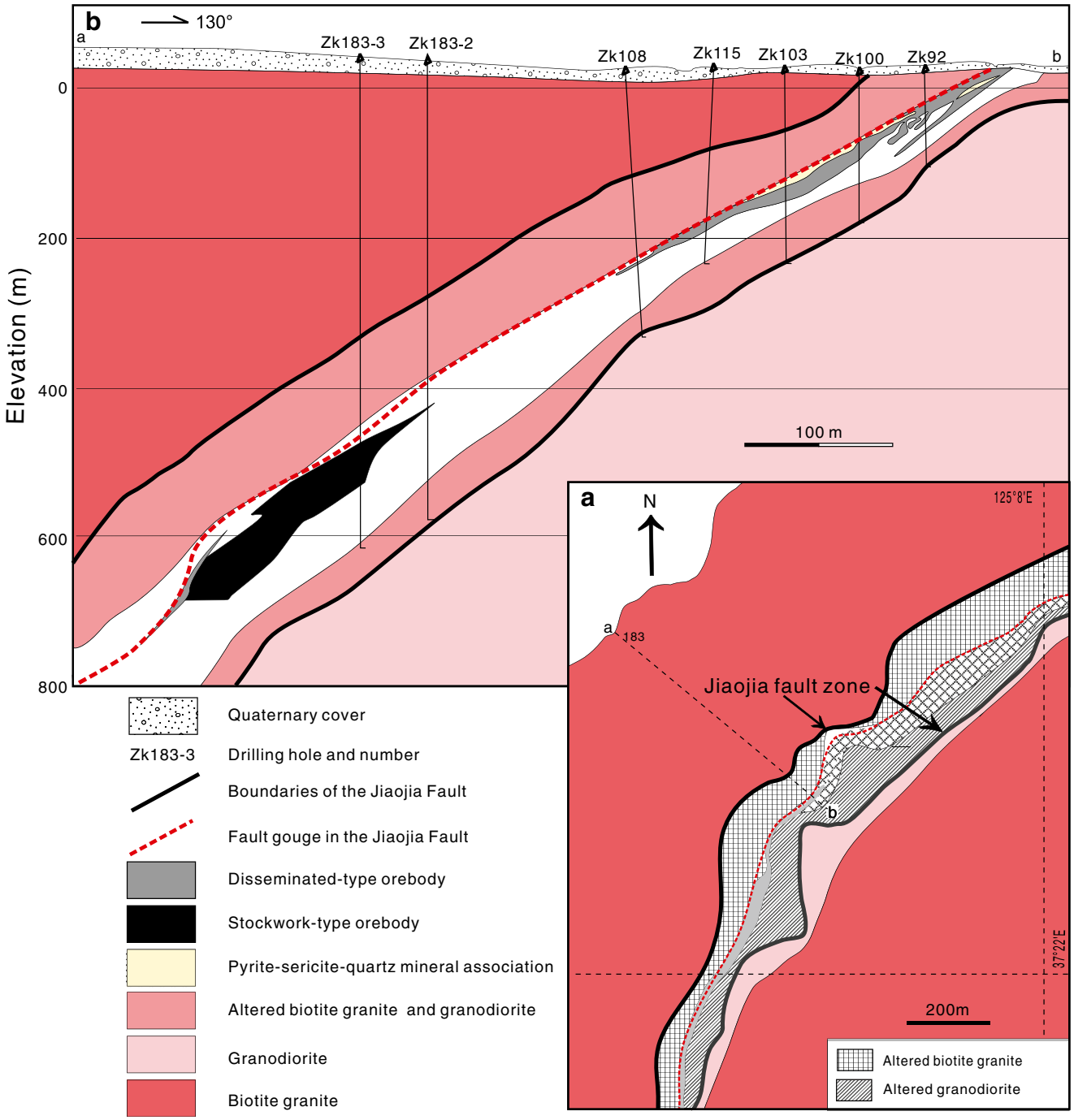

Fig. 4 Geological features of the Jiaojia Fault showing **a** the geological map of the Xincheng deposit and **b** geological section *a*–*b* in the #183 exploration line of the Xincheng deposit. The boundaries of the Jiaojia Fault represent extent of damage from large-scale brittle deformation (modified from Wang et al. 2015)

of 29 nA, and a 20-mA defocused electron beam. Apatite fission track dates were calibrated by the zeta-age calibration approach of Hurford and Green (1983) and are reported as central ages with ±2σ errors (95 % confidence interval). We used the χ^2 test to quantify age homogeneity; when P (χ^2)> 5 %, fission track samples contain a single age population (Galbraith 1981). For samples with P (χ^2)<5 %, we used binomial peak fitting to decompose the observed age distribution into best-fitting grain age components.

K–Ar dating

Fault gouge samples (XC480-01 and XC600-03) from the JJF at the Xincheng deposit (Fig. 6b, d) were analyzed for illite K–

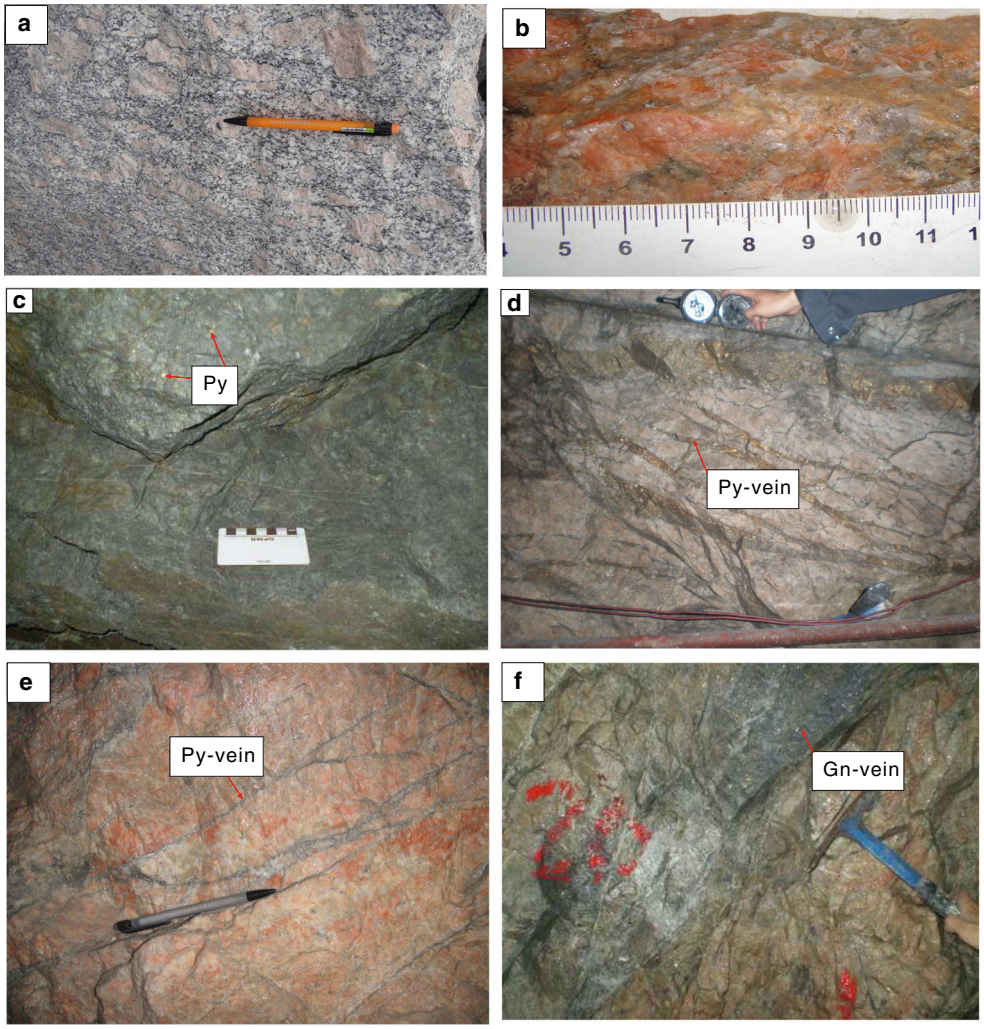

Fig. 5 Macroscopic features of samples selected for ore mineralogy and paragenetic studies of **a** Shangzhuang granodiorite, **b** K alteration of a granitic rock, **c** disseminated-type ore in quartz–sericite–pyrite-altered rocks, **d** stockwork-type ore in a silicified granitic rock, **e** stockwork-type ore in K-altered granitic rock, and **f** disseminated-type ore intersected by galena vein (modified from Wang et al. 2015)

Ar dating in order to constrain the timing of movements along the fault (Table 3). These samples consist of quartz, illite, illite/smectite, kaolinite, calcite, and pyrite. Results of X-ray diffraction analyses confirm that the clay mineral component along the JJF is dominantly illite/smectite (~73 %) with small amounts of saponite (~24 %) and minor amounts of kaolinite (~3 %) in the <0.15-μm fraction. The clay mineral component in the 0.15–0.3-μm fraction is, again, dominantly illite/smectite (~75 %) with small amounts of saponite (~20 %) and minor amounts of kaolinite (5 %). Similarly, major amounts of illite/smectite were found in the <0.3-μm fraction and minor amounts in the <2-μm fractions.

Illite separation was carried out using high-speed and super high-speed centrifugal separation techniques (Hamilton et al. 1989). The K–Ar dating technique follows the methods described in detail by Faure (1986). The argon isotopic composition of the JJF gouge samples was measured with an MM5400 Mass Spectrometer at the Center of Experiment and Research, China Research Institute of Petroleum Exploration and Development, Beijing. Illite samples were melted at 1500 °C and a quantitative diluent for ^{38}Ar was added. Subsequently, $(^{40}Ar/^{38}Ar)_m$, $(^{38}Ar/^{36}Ar)_m$, radioactive ^{40}Ar, and potassium contents were determined. The analytical error for the K/Ar age calculations is given at a 95 % confidence level (2σ).

Results

U–Pb dating

Zircons from the Shangzhuang granite are colorless or buff to transparent, euhedral to subhedral, and elongate to stubby grains. They display oscillatory zoning typical of magmatic grains in cathodoluminescence (CL) images (Fig. 7). The analytical results of the U–Pb dating are listed in Table 1. Data of Th/U ratios from the granodiorite samples vary between 0.24 and 0.83 also suggesting a magmatic origin (Table 1). Thus, the U–Pb ages of the zircons are interpreted as the crystallization ages of the rocks. The U–Pb concordia diagrams for the

Table 1 LA-ICP-MS zircon U–Pb analytical results in the Xincheng deposit

Spot no.	Content (ppm)			Th/U	Isotopic ratios								Apparent ages (Ma)	
	Pb	Th	U		$^{207}Pb/^{206}Pb$	(±1σ)	$^{207}Pb/^{235}U$	(±1σ)	$^{206}Pb/^{238}U$	(±1σ)	$^{208}Pb/^{232}Th$	(±1σ)	$^{206}Pb/^{238}U$	(±1σ)
SZ-02-1	46	104	376	0.28	0.04959	0.00038	0.13969	0.00137	0.02043	0.00014	0.00444	0.00033	130.4	0.9
SZ-02-2		80	268	0.30	0.05077	0.00081	0.14329	0.00252	0.02047	0.00019	0.00517	0.00050	130.6	1.2
SZ-02-4	37	68	236	0.29	0.05103	0.00165	0.14730	0.00504	0.02097	0.00097	0.00499	0.00216	133.8	6.2
SZ-02-6		76	214	0.35	0.05102	0.00075	0.14491	0.00221	0.02060	0.00015	0.00402	0.00055	131.5	0.9
SZ-02-7	58	74	235	0.31	0.04911	0.00482	0.13899	0.01245	0.02055	0.00020	0.00733	0.00122	131.1	1.3
SZ-02-8	37	75	218	0.35	0.04987	0.00053	0.14277	0.00171	0.02079	0.00018	0.00515	0.00039	132.7	1.2
SZ-02-9	35	103	213	0.48	0.05012	0.00050	0.14227	0.00166	0.02060	0.00016	0.00356	0.00027	131.5	1.0
SZ-02-10		368	627	0.59	0.05018	0.00032	0.14337	0.00146	0.02073	0.00018	0.00322	0.00015	132.3	1.1
SZ-02-11	40	109	287	0.38	0.05052	0.00052	0.14533	0.00176	0.02087	0.00016	0.00351	0.00031	133.2	1.0
SZ-02-12	24	71	159	0.45	0.04963	0.00138	0.14084	0.00516	0.02055	0.00037	0.00487	0.00069	131.1	2.4
SZ-02-13	96	254	378	0.67	0.05298	0.00056	0.15329	0.00178	0.02100	0.00015	0.00329	0.00017	134.0	0.9
SZ-02-14	68	174	333	0.52	0.05052	0.00039	0.14328	0.00139	0.02058	0.00015	0.00334	0.00019	131.3	0.9
SZ-02-15	47	113	323	0.35	0.05013	0.00038	0.14208	0.00129	0.02057	0.00014	0.00408	0.00024	131.3	0.9
SZ-02-16	36	90	267	0.34	0.05027	0.00035	0.14212	0.00122	0.02051	0.00013	0.00405	0.00027	130.9	0.8
SZ-02-17	37	92	229	0.40	0.04956	0.00046	0.14072	0.00150	0.02061	0.00015	0.00398	0.00029	131.5	0.9
SZ-02-18		141	312	0.45	0.05118	0.00056	0.14448	0.00185	0.02048	0.00017	0.00361	0.00028	130.7	1.1
SZ-02-19		273	446	0.61	0.04989	0.00030	0.14082	0.00129	0.02048	0.00016	0.00355	0.00018	130.7	1.0
SZ-02-20	40	84	214	0.39	0.04975	0.00046	0.14074	0.00164	0.02053	0.00017	0.00516	0.00036	131.0	1.1
XC480-03-1	9	54	121	0.44	0.04917	0.00210	0.13360	0.00574	0.01970	0.00022	0.00593	0.00103	125.7	1.4
XC480-03-2	20	53	158	0.34	0.04890	0.00233	0.13267	0.00647	0.01967	0.00029	0.00614	0.00228	125.5	1.8
XC480-03-3	27	73	227	0.32	0.05063	0.00113	0.13879	0.00329	0.01987	0.00018	0.00487	0.00060	126.8	1.1
XC480-03-4	48	90	281	0.32	0.05067	0.00040	0.13837	0.00144	0.01980	0.00015	0.00414	0.00032	126.4	1.0
XC480-03-5	28	85	333	0.26	0.05111	0.00059	0.14054	0.00184	0.01995	0.00017	0.00365	0.00037	127.3	1.1
XC480-03-6	21	65	206	0.32	0.05111	0.00084	0.14069	0.00275	0.01996	0.00022	0.00417	0.00049	127.4	1.4
XC480-03-7	87	131	295	0.45	0.04812	0.00315	0.13174	0.00697	0.01988	0.00032	0.00449	0.00078	126.9	2.0
XC480-03-8	32	77	270	0.28	0.05089	0.00061	0.13867	0.00202	0.01976	0.00018	0.00384	0.00034	126.1	1.1
XC480-03-9	86	168	476	0.35	0.05126	0.00042	0.14111	0.00145	0.01999	0.00017	0.00320	0.00023	127.6	1.1
XC480-03-10	235	478	577	0.83	0.05067	0.00039	0.14008	0.00154	0.02006	0.00018	0.00305	0.00021	128.1	1.1
XC480-03-11	36	58	173	0.34	0.05099	0.00183	0.13896	0.00506	0.01976	0.00031	0.00445	0.00076	126.2	1.9
XC480-03-12	114	234	668	0.35	0.04933	0.00149	0.13557	0.00357	0.01994	0.00024	0.00304	0.00052	127.3	1.5
XC480-03-14	40	78	233	0.33	0.05076	0.00056	0.13962	0.00155	0.01998	0.00013	0.00432	0.00037	127.5	0.8
XC480-03-15	93	168	459	0.36	0.05125	0.00040	0.14168	0.00136	0.02007	0.00015	0.00373	0.00023	128.1	0.9
XC480-03-16	29	69	189	0.37	0.05113	0.00075	0.13923	0.00216	0.01976	0.00015	0.00409	0.00044	126.1	1.0
XC480-03-17		96	366	0.26	0.04961	0.00040	0.13605	0.00127	0.01991	0.00012	0.00375	0.00025	127.1	0.8

Table 1 (continued)

Spot no.	Content (ppm)			Th/U	Isotopic ratios								Apparent ages (Ma)	
	Pb	Th	U		$^{207}Pb/^{206}Pb$	(±1σ)	$^{207}Pb/^{235}U$	(±1σ)	$^{206}Pb/^{238}U$	(±1σ)	$^{208}Pb/^{232}Th$	(±1σ)	$^{206}Pb/^{238}U$	(±1σ)
XC480-03-18	39	93	268	0.34	0.05068	0.00057	0.13981	0.00168	0.02002	0.00013	0.00369	0.00028	127.8	0.9
XC480-03-19	111	208	525	0.40	0.05116	0.00049	0.14243	0.00176	0.02017	0.00014	0.00374	0.00022	128.7	0.9
XC480-03-20	68	95	337	0.28	0.04990	0.00108	0.13631	0.00267	0.01981	0.00011	0.00507	0.00121	126.5	0.7

zircon analyses are shown in Fig. 7. Eighteen of 20 zircon analyses from sample SZ-02 form a tight cluster, with a weighted mean $^{206}Pb/^{238}U$ age of 132±1 Ma (2σ, mean square of weighted deviation (MSWD)=0.9; Fig. 7a). Nineteen of 20 analyses of zircons from sample XC480-03 also form a tight cluster, close to concordia, with a weighted mean $^{206}Pb/^{238}U$ age of 127±1 Ma (2σ, MSWD=0.6; Fig. 7b).

Fission track dating

The data for ore samples with $P(\chi^2)>5$ % are characteristic of normal single grain age distribution (Fig. 8), yielding central ages between 55 and 21 Ma. The track length distribution is unimodal positively skewed and relatively narrow (Fig. 9). The mean track length is short (12.3 μm), which is typical of rocks with repetitive stay within or slow cooling through the apatite partial annealing zone (~60–120 °C; Tagami and Shimada 1996).

Illite K–Ar dating

Sample XC480-01 yielded illite K–Ar ages of 83±2 and 68±2 Ma. Sample XC600-03 yielded illite K–Ar ages of 85±1 and 82±2 Ma. The radiogenic ^{40}Ar content of these samples ranges from 68.0 to 90.4 %, which indicates that the results are reliable. The potassium contents range from 5.15 % (<0.15 μm) to 5.72 % (0.3–0.15 μm). The related nearly identical K–Ar data for these size fractions suggest similar illite formation ages, because other K-rich mineral contaminants could not be detected by XRD investigations. Another K-feldspar has been identified in the 2–6-μm fractions in some samples, but none has been found in the <0.15-μm fraction (Table 3). Illite is of authigenic origin and, therefore, represents a negligible source of error for the age interpretations.

Discussion

Tectonic evolution of the Jiaojia Fault

Jurassic initiation and sinistral movement

The Jurassic (ca. 160–150 Ma) Linglong Granite bordering the JJF (Figs. 2 and 3) has been interpreted as having been derived by partial melting of a tectonically thickened crust (Wang et al. 1998; Qiu et al. 2002; Hu et al. 2004; Guo et al. 2005). Their ages have been determined by SHRIMP/LA–ICP–MS U–Pb zircon method to be at 160±3 to 153±4 Ma (Miao et al. 1997; Wang et al. 1998), 157±2 Ma (Zhang et al. 2010), 159±1 Ma (Yang et al. 2012), and 160±3 to 157±3 Ma (Ma et al. 2013).

Table 2 Apatite fission track analytical data of the Xincheng gold deposit samples

Sample	No. of grains	Rock type	ρ_s (10^5/cm^2) (Ns)	ρ_i (10^5/cm^2) (Ni)	ρ_d (10^5/cm^2) (N)	P (χ^2)	L (μm) (N)	Central age (Ma) (±1σ)	Pooled age (Ma) (±1σ)
SC-01	35	Ore	0.846 (190)	4.837 (1086)	16.37 (10,405)	7.0	12.1±2.0 (39)	55±6	56±5
XC175-02	31	Ore	1.336 (474)	9.762 (3464)	16.768 (10,405)	8.2	12.7±2.1 (73)	44±3	45±3
XC205-04	28	Ore	0.373 (94)	5.813 (1464)	16.968 (10,405)	68.3	11.1±1.5 (4)	21±3	21±3
XC480-03	28	Ore	0.587 (264)	4.911 (2208)	17.167 (10,405)	6.0	12.8±2.0 (93)	40±4	40±3
XC480-07	20	Ore	0.415 (81)	5.005 (977)	17.366 (10,405)	8.4	13.0±2.1 (88)	28±4	28±4
XC580-18	28	Ore	0.654 (209)	5.54 (1770)	18.362 (10,405)	77.1	12.0±2.2 (70)	42±4	42±4
XC600-07	28	Ore	0.761 (177)	5.846 (1359)	18.96 (10,405)	95.2	12.3±2.0 (37)	48±5	48±5
XC600-08	32	Ore	0.546 (155)	5.787 (1644)	19.159 (10,405)	9.8	12.7±2.0 (83)	35±4	35±3

ρ_s spontaneous track density of a sample, *Ns* number of tracks counted to determine ρ_s, ρ_i induced track density of a sample measured in a muscovite external detector, *Ni* number of tracks counted to determine ρ_i, ρ_d induced track density of glass dosimeter measured in a muscovite external detector, N_d number of tracks counted to determine ρ_d, T fission track age with its 1σ error, n number of crystals counted; $P(\chi^2)$ probability of obtaining the observed value of χ^2 parameter, for N degree of freedom, where N=(number of counted crystals)−1

Various researchers have attempted to explain the tectonic setting for the Jurassic magmatism in the Jiaodong Peninsula, but a consensus has not been reached (Zhou and Lu 2000; Wang et al. 2013). However, most researchers consider that the collision between the North China and Yangtze cratons commenced in the latest Paleozoic to Early Mesozoic and ended by the Early Jurassic (ca. 213–188 Ma) (Okay and Sengor 1992; Yin and Nie 1993; Li 1994). Since the Middle Jurassic, the Paleo-Pacific Plate subducted beneath the NCC resulting in adakite-like magmatism in an active compressive continental margin (Wu et al. 2005; Wang et al. 2014c), such as the Linglong Granite in the Shandong Peninsula (Wu et al. 2005). Therefore, we interpret the U–Pb results in the context of the convergence between the Paleo-Pacific oceanic plate and the Asian continent.

Previous researchers have suggested that a sinistral shear on the NE striking faults under a NNW–SSE compression, while WSW–ENE tension may have taken place during the Early–Middle Jurassic (Xu et al. 1987; Gilder et al. 1999; Schmid et al. 1999; Mercier et al. 2007). This resulted in sinistral transform faults in the Jiaodong Peninsula (Fig. 10a). Zhu et al. (2004) have reported that $^{40}Ar/^{39}Ar$ plateau ages of muscovite samples of mylonite from a sinistral ductile shear zone are ca. 193–189 Ma, suggesting that a sinistral strike–slip movement has taken place in the Early Jurassic along the Tan-Lu Fault. In addition, we observed domino-type structures along the JJF (Fig. 6b), which are indicative of sinistral shearing during the Jurassic. As mentioned earlier, during the Early–Middle Jurassic and possibly the Late Jurassic, the NE-trending faults have acted as sinistral transform faults (Fig. 10a).

Early Cretaceous switch between normal and sinistral strike–slip faulting

The Cretaceous magmatism is represented by the emplacement age of the Shangzhuang granite bordering the JJF (Fig. 3), with U–Pb zircon ages of 130±3 to 126±2 and 129±1 Ma (Hu et al. 1987; Xu et al. 1989; Li and Yang 1993; Miao et al. 1997; Wang et al. 1998, 2014d; Yang and Zhou 2001; Yang et al. 2012). Our zircon LA-ICP-MS U–Pb dating of the granodiorite from the JJF yield interpreted emplacement ages of ca. 132 and 127 Ma, consistent with previous dating (Fig. 7). The granodiorite is interpreted to be related to the subduction of the Paleo-Pacific Plate beneath the NCC, which was possibly associated with slab break-off and roll back or lithospheric delamination of the NCC (Xu et al. 2009; Yang et al. 2012; Zhang et al. 2014; Wilde et al. 2003; Zhai and Santosh 2013). This magma emplacement was aided by the development of the NE-trending faults (Guo et al. 2014).

The ages of the igneous rocks constrain on the age of the NNE-trending normal faults in the Jiaodong Peninsula that resulted from a NW–SE tension and a NE–SW compression lasting from 135 to 120 Ma (Fig. 10b; Xu and Zhu 1994; Zhang et al. 2003a, b; Zhu et al. 2004; Ren et al. 2007; Sun et al. 2007; Deng et al. 2009a). Charles et al. (2011) and Yang et al. (2014) report that the NNE-trending Zhaoping Fault, which hosts the Zhaoyuan and Dayingezhuang gold deposits, is a detachment fault related to major extensional tectonics. This was followed by sinistral strike–slip faulting associated compression orientated NW–SE and NE–SW orientated tension at ca. 120–110 Ma (Fig. 10c; Sun et al. 2007; Mercier et al. 2007). This was followed at ca. 110 Ma with a change in the strain field with normal faulting related to ENE–SWW compression and a NNW–SSE tension (Zhu et al. 2004; Sun et al. 2007; Mercier et al. 2007). The volcanic rocks in the Laiyang Basin to the north of the Sulu Belt were erupted at ca. 110–105 Ma during that period (Fig. 10d; Qiu et al. 2001b; Guo et al. 2005).

Late Cretaceous–Paleocene normal faulting

Previous authors have attempted to explain the formation, age, and dynamic characteristics of the normal Tan-Lu Fault and its

Table 3 K–Ar dating data for illites from the Jiaojia Fault

Sample no.	Grain-size fraction (μm)	Montmorillonite (%)	I/S (%)	Illite (%)	Kaolinite (%)	Chlorite (%)	K-feldspar	K (%)	$(^{40}Ar/^{38}Ar)_m$	$(^{38}Ar/^{36}Ar)_m$	$^{40}Ar_{rad}$ (mol/g)	$^{40}Ar_{rad}$ (%)	^{40}K (^{40}K/g) (mol/g)	Age (Ma, 1σ)
XC480-01	<2	No	19	78	3	No	No							
XC480-01	0.3–0.15	22	75	No	3	No	No	5.28	228.02351	3.79128	7.802E-10	68.26	1.576E-07	83.3±2.1
XC480-01	<0.15	28	70	No	2	No	No	5.72	195.32851	4.45984	6.868E-10	68.00	1.707E-07	67.9±1.7
XC600-03	<2	no	14	76	3	7	No							
XC600-03	0.3–0.15	18	75	No	7	No	No	5.52	197.66435	15.85584	8.385E-10	90.37	1.648E-07	85.5±0.8
XC600-03	<0.15	21	75	No	4	No	No	5.15	224.17468	4.44469	7.507E-10	72.40	1.537E-07	82.2±1.7

subsidiary NNE-trending structures during the Late Cretaceous–Paleocene in the Jiaodong Peninsula (Wan and Zhu 1996; Faure et al. 1999; Grimmer et al. 2002; Zhu et al. 2004; Mercier et al. 2007; Deng et al. 2009a, b). Wan and Zhu (1996) and Wang et al. (2009) suggest that the fault was active during the Late Cretaceous which was a normal fault with minor sinistral strike–slip movement. As the fault is bordered by a half graben filled with Late Cretaceous to Paleocene sediments, the extensional tectonics related to the normal faulting is regarded as being Late Cretaceous–Paleocene in age (Xu 1993; Zhu et al. 2000). Our illite K–Ar ages of 86±1 and 68±2 Ma along the JJF correspond to this period of extensional faulting along the NNE-trending structures in the peninsula. The subduction direction of the Paleo-Pacific Plate changed again by ~75° from NEE–SWW to NW–SE, which resulted in the change from ENE–WSW compression and NNW–SSE tension during the late Early Cretaceous to NNE–SSW compression and WNW–ESE tension during the Late Cretaceous to Paleocene (Sun et al. 2007). This change happened after 94±5 Ma, based on the K/Ar illite isotopic data of fault gouge in a northern segment of the Tan-Lu Fault Zone (Koppers et al. 2001; Wang et al. 2009). This interpretation is supported by the change from a late Early Cretaceous NW–SE compression in the Yi–Shu Rift to a Late Cretaceous~N–S tension in the Jiaolai Graben during 100–90 Ma (Fig. 10e; Zhang et al. 2003a, b; Wang et al. 2009).

Eocene–Oligocene dextral movement and normal faulting

The variable apatite fission track age, the track length distribution, and thermal models suggest that the JJF experienced two major cooling stages caused by exhumation (Fig. 11). These stages relate to (1) a slow exhumation/cooling and uplift in response to a small magnitude of initial extensional deformation during ca. 55 Ma or earlier and (2) a rapid exhumation/cooling and uplift in response to a large magnitude of accelerated extensional deformation initiated at ca. 25 Ma.

Our apatite fission track data analysis and thermal modeling of representative samples dated at ca. 55 Ma corresponds to this period of dextral movement and normal faulting along the NNE-trending structures in the Jiaodong Peninsula. Along the JJF, we observed quartz veins cut by dextral shear in quartz–sericite–pyrite-altered rocks (Fig. 6c). Formation of Eocene rift basins in the Jiaodong Peninsula has been documented at ca. 55 Ma during NW–SE dextral transtension (Fig. 10f; Yan and Ma 1992; Allen et al. 1997; Ren et al. 2007; Huang et al. 2013). It is commonly thought that the Eocene strike–slip and normal faults in the Jiaodong Peninsula are the result of extrusion tectonics driven by the subduction of the Pacific Plate underneath the NCC (Chen and Dickinson 1986; Northrup et al. 1995). Others suggest that the intracontinental deformation in the Jiaodong Peninsula can be

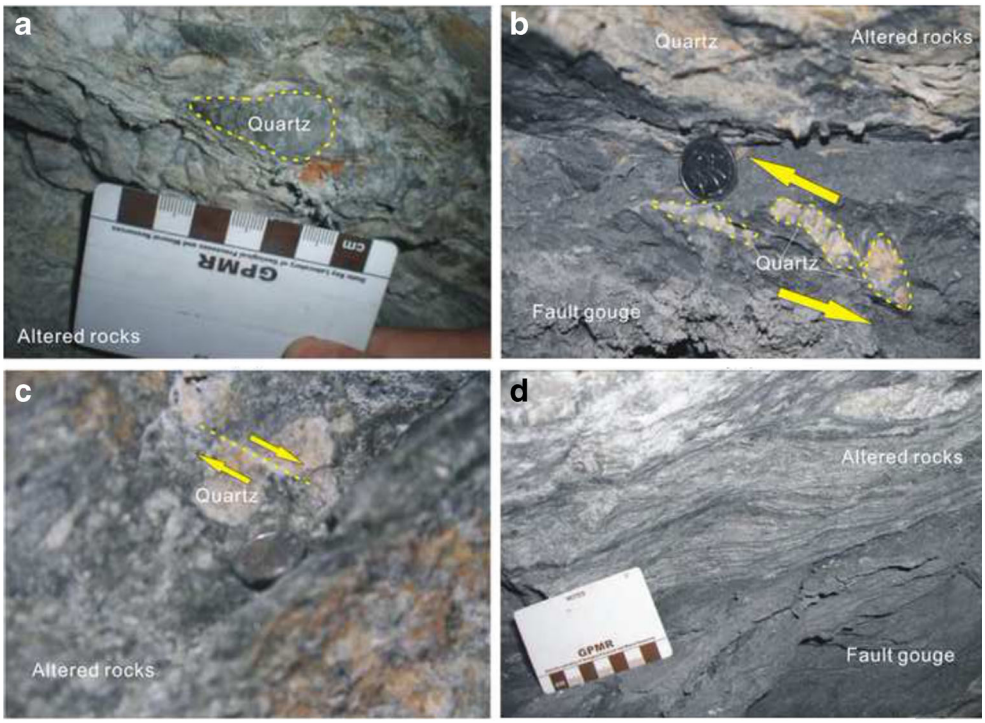

Fig. 6 Macroscopic features of the Jiaojia Fault: **a** augen structure of quartz, **b** domino structure, **c** quartz cut by dextral shear, and **d** schistosity zone

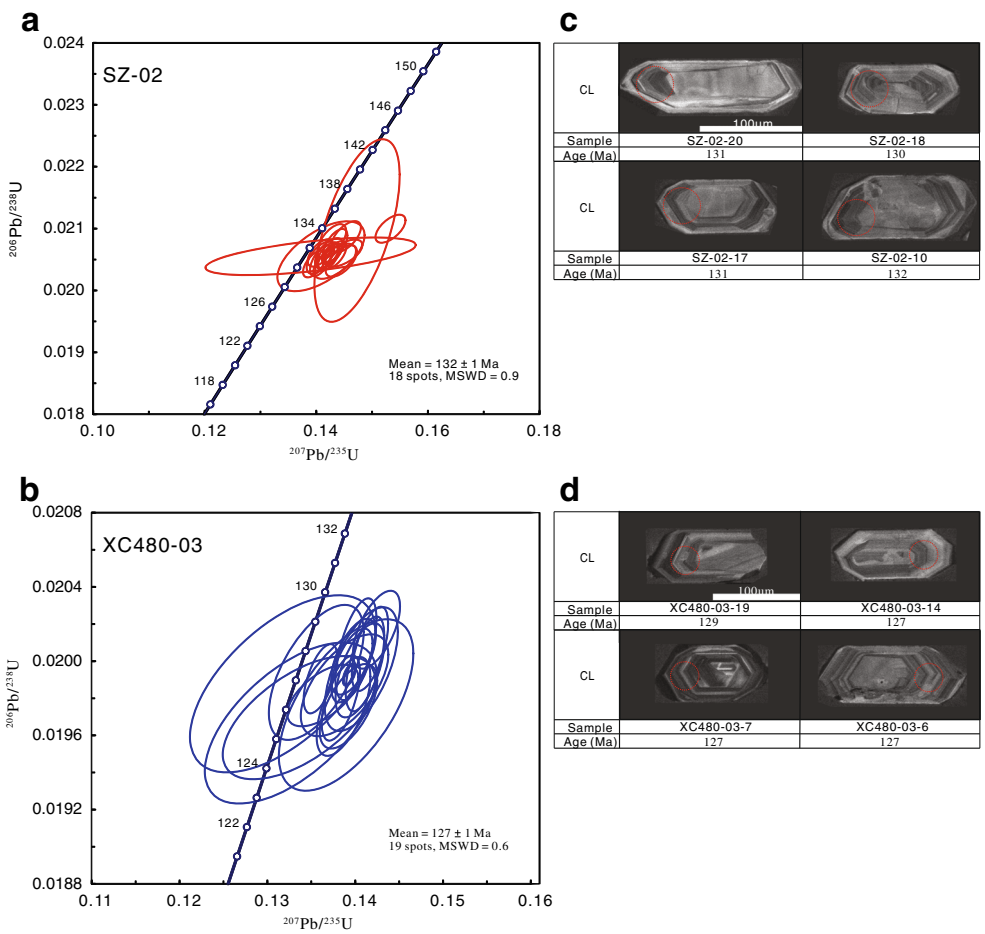

Fig. 7 Zircon U–Pb concordia plots and calculated weighted mean $^{206}Pb/^{238}U$ dates for Shangzhuang granite from the Xincheng gold deposit

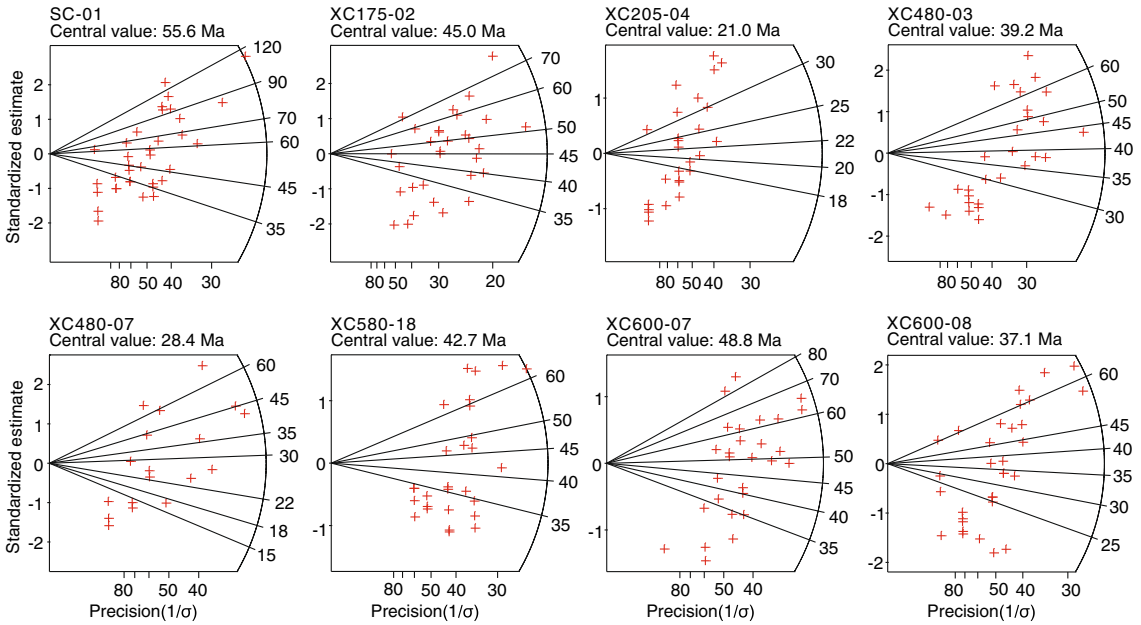

Fig. 8 Radial plots of single grain apatite ages with extra Poissonian variations. The *Y*-axis indicates the standardized error on single grain ages, and the *X*-axis depicts the percentage of relative error (inversely related to precision) of each grain age. Single grain ages are read off the axis (plotted on a logarithmic scale) by drawing a line through the single grain point from the intercept to the radial scale

linked to the far-field effects of the interaction of the Indian subcontinent with the Eurasian continent during 65–55 Ma (Grimmer et al. 2002; Ratschbacher et al. 2003; Deng et al. 2014a, b; Wang et al. 2014a, b). However, the Indo-Asian collision has little effect on lithospheric evolution of the North China Craton (Zheng et al. 2006; Huang et al. 2011). We propose that the Eocene dextral movement along the NNE-trending structures is a consequence of a change in the movement direction of the Paleo-Pacific Plate from NNE–SSW to its present direction of NW–SE (Beck et al. 1995; Sharp and Clague 2006; Sun et al. 2007).

A regional Late Oligocene inversion associated with a regional ca. 25 Ma unconformity at the base of Neogene strata is documented from the East China Sea and the Jianghan, Hehuai, Jiangsu, Bohai, and Songliao basins (Chen et al. 1989; Hu et al. 1987; Allen et al. 1997). Neogene thermal subsidence in the basins was accompanied by minor normal faulting lasting until the present day (Allen et al. 1997; Gilder et al. 1991; Grimmer et al. 2002).

Tectonic transition and large-scale gold mineralization

The determination of the mineralization age for gold deposits along the JJF is critical for the understanding of its relationship to the tectonic evolution of the NNE-trending structures in the Jiaodong Peninsula. K-feldspar separates from the Dongji deposit have an Ar/Ar plateau age of ca. 116 Ma (Li et al. 2003b). Sericite and muscovite separates from the Jiaojia, Xincheng, and Wang'ershan deposits have Ar/Ar plateau ages of ca. 120 to 119 Ma, ca. 121 to 120 Ma, and ca. 121 to

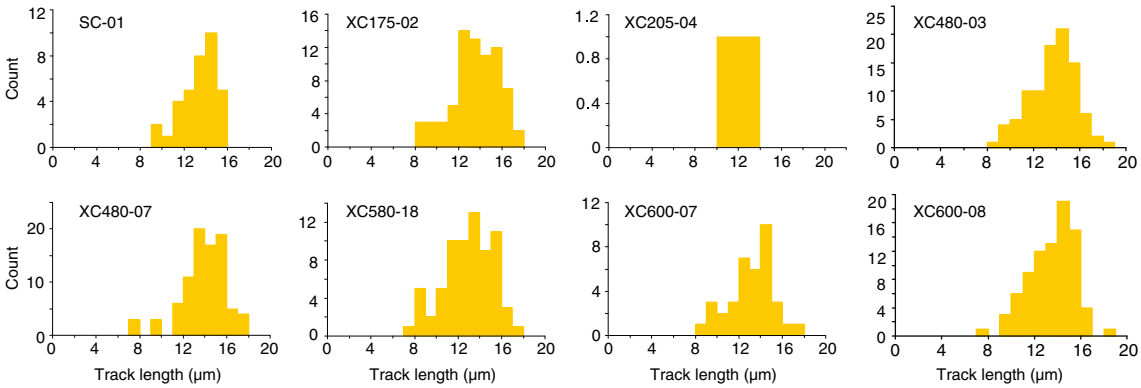

Fig. 9 Histogram of the apatite fission track ages

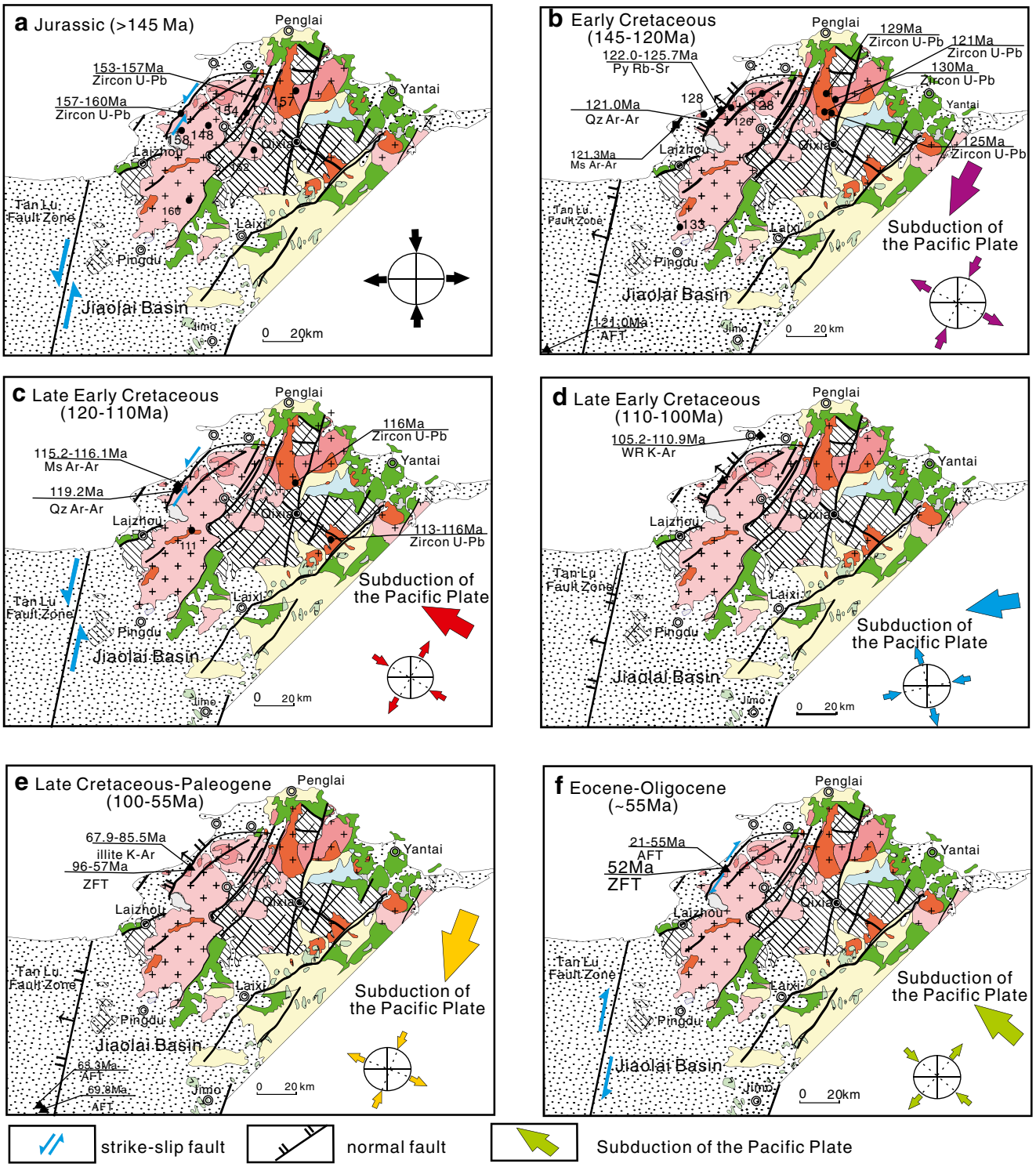

Fig. 10 Evolution of regional stress field and kinematic model of the middle Tan-Lu Fault Zone and NNE-trending structures in the Zhaoyuan–Laizhou area. The drifting history of the Pacific Plate is based on Koppers et al. (2001) and Sun et al. (2007). Evolution of the middle Tan-Lu Fault Zone and Jiaojia Fault after Chen and Dickinson (1986), Xu et al. (1987), Yan and Ma (1992), Northrup et al. (1995), Wan and Zhu (1996), Allen et al. (1997), Faure et al. (1999), Gilder et al. (1999), Schmid et al. (1999), Grimmer et al. (2002), Zhang et al. (2003a, b), Zhu et al. (2004), Sharp and Clague (2006), Ren et al. (2007), Mercier et al. (2007), Sun et al. (2007), Deng et al. (2009a), Wang et al. (2009), Charles et al. (2013), Gu et al. (2013), and Huang et al. (2013)

119 Ma, respectively (Li et al. 2003a). Two Rb–Sr ages of ca. 126±6 and 122±7 Ma were obtained by Wang et al. (2015) from pyrite sampled from the Xincheng gold deposit. Previous dating using the Rb–Sr and Ar–Ar techniques on

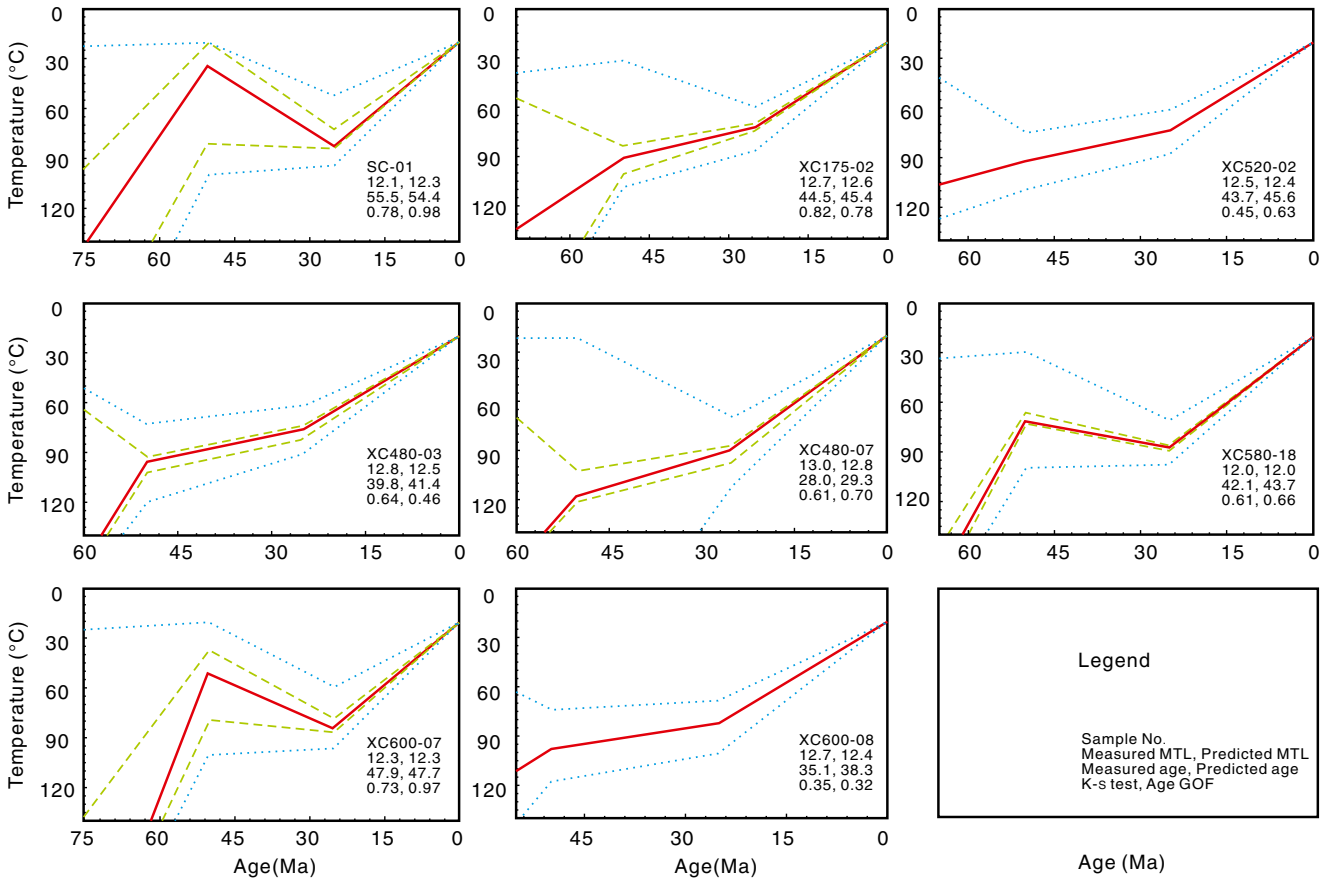

Fig. 11 Time–temperature histories of samples from the Jiaojia Fault calculated by inverse modeling observed apatite fission track parameters, based on the annealing model of Ketcham et al. (1999). The *X*- and *Y*-coordinate reflect the fission track age (Ma) and the temperature (°C), respectively. Shown at the *bottom right of each panel* is the sample number, measured and model predicted track length, measured and modeled pooled age, and Kolmogorov–Smirnov test, which is used to determine similarity between the measured and predicted apatite fission track age and length parameters. Field between *dot lines* is the acceptable result predicted by the model, the *dashed line space* is the goodness-of-fit result, and the *solid line* is the best-fit result

alteration minerals and fluid inclusions in quartz indicate that the timing of the gold mineralization along the NNE-trending structures in the peninsula is between 130 and 110 Ma (Yang et al. 2003; Li et al. 2013; Zhai and Santosh 2013). The Rb–Sr isochron ages of sericite and pyrite from the Linglong gold deposit along the Zhaoyuan Fault are 112±2 and 120±1 to 123±4 Ma (Luo and Wu 1987; Li et al. 2008) and 120±4 to 123±4 Ma (Yang 2000; Yang and Zhou 2001), respectively. The Ar/Ar plateau age for muscovite from the Sanshandao Fault at the Cangshang deposit is ca. 121 Ma (Zhang et al. 2003a, b. These dates show that the age of gold mineralization in this area is between ca. 130 and 110 Ma, which coincides with the Early Cretaceous magmatism and the transition from early Early Cretaceous (145–120 Ma) normal faulting to late Early Cretaceous (120–110 Ma) sinistral strike–slip faulting (Figs. 10b, c and 12a, b).

In addition, based on these dates, the gold mineralization is correlated with extensive lithospheric thinning that took place at ca. 120 Ma in the Jiaodong Peninsula (Deng et al. 2015). This took place in a period when the stress field in eastern China changed from extension to transpression, resulting from the near orthogonal change in the subduction direction of the Paleo-Pacific Plate from NE–SW to NW–SE (Fig. 10b, c; Koppers et al. 2001; Sun et al. 2007). The transitions of the subduction direction synchronized the lithosphere thinning and the change from normal to sinistral movement along NNE-trending faults that host gold deposits (Fig. 10b, c). Thus, the tectonic setting of the gold deposits in JJF is markedly different from those defined for typical orogenic gold deposits at convergent plate margins (Groves et al. 1998). The geodynamic engine of the Jiaodong gold deposits is the lithospheric thinning and structure adjustment induced by Pacific slab subduction, and the gold mineralization in the Jiaodong Peninsula belongs to intraplate metallogeny. Instead, we propose that these deposits constitute a unique class of "Jiaodong-type" gold deposits, as proposed by earlier researchers (Zhai et al. 2004; Zhai and Santosh 2013; Song et al. 2014; Deng et al. 2015; Li et al. 2015).

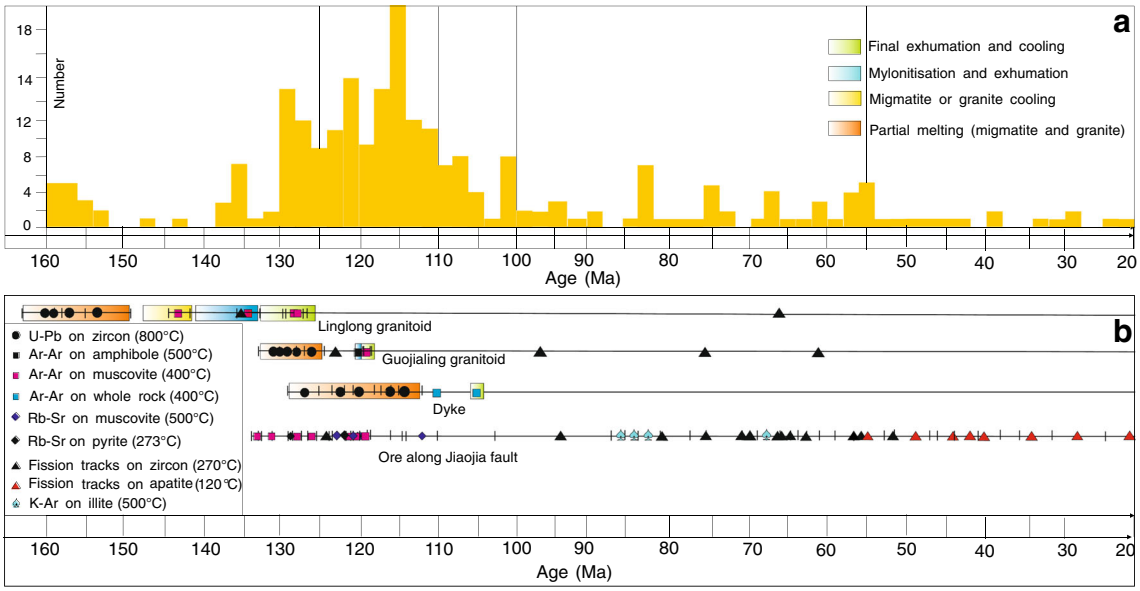

Fig. 12 Summary of geochronological data and tectonic history showing **a** histogram of the recent high precision dating results from SHRIMP and LA–ICP–MS zircon U–Pb ages, zircon and apatite fission track data, and $^{40}Ar/^{39}Ar$ ages in the Jiaodong Peninsula; and **b** the timing of magmatism and thermal events in the Zhaoyuan–Laizhou area (modified from Wang et al. 2015). Major data sources: Hu et al. (1987), Hu et al. (2004), Hu et al. (2007), Chen et al. (1988), Xu et al. (1989), Li and Yang (1993), Miao et al. (1997), Wan and Wang (1997), Zhao et al. (1997), Guan et al. (1998), Wang et al. (1998, 2005), Qiu et al. (2001a, b, 2012), Yang and Zhou (2001), Zhang et al. (2002, 2010), Zhou et al. (2003), Guo et al. (2004, 2005), Li et al. (2006), Ling et al. (2006), Liu et al. (2004, 2008, 2009), Tan et al. (2008), Tang et al. (2004, 2008), Xie et al. (2008), Goss et al. (2010), Yang et al. (2005, 2012), Kuang et al. (2012), Charles et al. (2013), Ma et al. (2013), Yang et al. (2014), and this study. Mean mineral closure temperatures are from Tagami and Shimada (1996), Villa (1998), Yang (2000), and Verdel et al. (2012)

Conclusions

1. LA-ICP-MS U–Pb zircon ages of ca. 132±1 and 127±1 Ma from granites constrain that the JJF was a normal fault during the Early Cretaceous, corresponding to a period of large-scale lode gold mineralization, extension-related magmatism, and Cretaceous giant igneous events in the Jiaodong area.
2. This sinistral strike–slip faulting of the JJF lasted during ca. 120–110 Ma, which was related to NW–SE compression and NE–SW tension.
3. Illite K–Ar dates of ca. 83±2 to 68±2 Ma constrain the timing of a second normal faulting event along the JJF (with the first being ca. 110 Ma and the last being ca. 55 Ma).
4. Measured apatite fission track ages of between 55 and 21 Ma correspond to a dextral movement along the JJF.
5. Large-scale gold mineralization is related to a transition of NNE-trending structures from early Early Cretaceous normal faulting to late Early Cretaceous sinistral strike–slip faulting, providing important evidence for the tectonic setting of the Jiaodong gold deposits.

Acknowledgments This research was jointly supported by the National Natural Science Foundation of China (No. 41230311), the Fundamental Research Funds for the Central Universities (No. 2652013034), the China Minmetals Corporation Program (No. 2013KC0201), and the 111 Project (No. B07011). The authors thank the team members, including Professors Wanming Yuan, Liqiang Yang, Qingfei Wang, and Qingjie Gong and associate Professors Jin Zhang and Xuefei Liu, from the China University of Geosciences in Beijing, for the field research, constructive discussions, and comments. This is contribution 582 from the ARC Centre of Excellence for Core to Crust Fluid Systems (www.CCFS.mq.edu.au). The authors are deeply indebted to Dr. Thomas Bissig and the anonymous journal reviewers for their critical reviews and constructive comments.

References

Allen MB, Macdonald DIM, Xun Z, Vincent SJ, Brouet-Menzies C (1997) Early Cenozoic two-phase extension and late Cenozoic thermal subsidence and inversion of the Bohai Basin, northern China. Mar Pet Geol 14:951–972

Beck RA, Burbank DW, Sercombe WJ, Riley GW, Barndt JK, Berry JR, Afzal J, Khan AM, Jurgen H, Metje J, Cheema A, Shafique NA, Lawrence RD, Khan MA (1995) Stratigraphic evidence for an early collision between Northwest India and Asia. Nature 373:55–58

Charles N, Gumiaux C, Augier R, Chen Y, Zhu RX, Lin W (2011) Metamorphic core complexes vs. synkinematic plutons in continental extension setting: insights from key structures (Shandong Province, eastern China). J Asian Earth Sci 40:261–278

Charles N, Augier R, Gumiaux C, Monié P, Chen Y, Faure M, Zhu RX (2013) Timing, duration and role of magmatism in wide rift systems: insights from the Jiaodong Peninsula (China, East Asia). Gondwana Res 24:412–428

Chen Q, Dickinson WR (1986) Contrasting nature of petroliferous Mesozoic–Cenozoic basins in eastern and western China. Am Assoc Pet Geol Bull 70:263–275

Chen WJ, Ji FJ, Li Q, Li DM, Wang QL, Wang X (1988) Eochronological implication of K-Ar, FT, and TL system of fault gouge from Yi-Shu fault zone. Seismol Geol Res 10:191–198

Chen GY, Shao W, Sun DS (1989) Genetic mineralogy and prospecting of Jiaodong gold deposits. Chongqing Publishing House, Chongqing, pp 1–234, in Chinese with English abstract

De Boorder H (2015) The Jiaodong gold district, northeastern China, in the context of the Late Paleozoic and Late Mesozoic large igneous provinces, orogeny and metallogeny in Eurasia. Ore Geol Rev 65: 574–588

Deng J, Yang LQ, Sun ZS, Wang JP, Wang QF, Xin HB, Li XJ (2003) A metallogenic model of gold deposits of the Jiaodong granite–greenstone belt. Acta Geol Sin 77:537–546

Deng J, Yang LQ, Ge LS, Wang QF, Zhang J, Gao BF, Zhou YH, Jiang SQ (2006) Research advances in the Mesozoic tectonic regimes during the formation of Jiaodong ore cluster area. Prog Nat Sci 16: 777–784

Deng J, Wang QF, Li W, Gong QJ, Zhao J, Liu H (2009a) Self-similar fractal analysis of gold mineralization of Dayingezhuang disseminated-veinlet deposit in Jiaodong gold province, China. J Geochem Explor 102(2):95–102

Deng J, Yang LQ, Gao BF, Sun ZS, Guo CY, Wang QF, Wang JP (2009b) Fluid evolution and metallogenic dynamics during tectonic regime transition: example from the Jiapigou Gold Belt in Northeast China. Resour Geol 59:140–152

Deng J, Wang QF, Li GJ, Li CS, Wang CM (2014a) Tethys evolution and spatial-temporal distribution of ore deposits in the Sanjiang region, southwestern China. Gondwana Res 26:419–437

Deng J, Wang QF, Li GJ, Santosh M (2014b) Cenozoic tectono-magmatic and metallogenic processes in the Sanjiang region, southwestern China. Earth Sci Rev 138:268–299

Deng J, Liu XF, Wang QF, Pan RG (2015) Origin of the Jiaodong-type Xinli gold deposit, Jiaodong Peninsula, China: constraints from fluid inclusion and C–D–O–S–Sr isotope compositions. Ore Geol Rev 65:674–686

Fan HR, Zhai MG, Xie YH, Yang JH (2003) Ore-forming fluids associated with granite hosted gold mineralization at the Sanshandao deposit, Jiaodong gold province, China. Miner Deposita 38:739–750

Faure G (1986) Principles of isotope geology. Wiley, New York, p 589

Faure M, Lin W, Shu LS, Sun Y, Schärer U (1999) Tectonics of the Dabie Shan (eastern China) and possible exhumation mechanism of ultrahigh pressure rocks. Terra Nova 11(6):251–258

Galbraith RF (1981) On statistical models for fission track counts. Math Geol 13:471–488

Gilder S, Keller GR, Luo M, Goodell PC (1991) Timing and spatial distribution of rifting in eastern China. Tectonophysics 197:225–243

Gilder SA, Leloup PH, Courtillot V, Chen Y, Coe RS, Zhao XX, Xiao WJ, Halim N, Cogné JP, Zhu RX (1999) Tectonic evolution of the Tangcheng–Lujiang (Tan–Lu) fault via middle Triassic to Early Cenozoic Paleomagnetic data. J Geophys Res 104(B7):15365–15390

Goldfarb RJ, Groves DI, Gardoll S (2001) Orogenic gold and geological time: a global synthesis. Ore Geol Rev 18:1–73

Goldfarb RJ, Baker T, Dube B, Groves DI, Hart CJR, Robert F, Gosselin P (2005) Distribution, character, and genesis of gold deposits in metamorphic terranes. 100th Anniversary Volume of Economic Geology, pp. 407–450

Goldfarb RJ, Hart CJR, Davis G, Groves DI (2007) East Asian gold—deciphering the anomaly of Phanerozoic gold in Precambrian cratons. Econ Geol 102:341–346

Goldfarb RJ, Taylor RD, Collins GS, Goryachev NA, Orlandini OM (2014) Phanerozoic continental growth and gold metallogeny. Gondwana Res 25:48–102

Goss SC, Wilde SA, Wu F, Yang J (2010) The age, isotopic signature and significance of the youngest Mesozoic granitoids in the Jiaodong Terrane, Shandong Province, North China Craton. Lithos 120: 309–326

Grimmer JC, Jonckheere R, Enkelmann E, Ratschbacher L, Hacker BR, Blythe AE, Wagner GA, Wu Q, Liu S, Dong S (2002) Cretaceous-Cenozoic history of the southern Tan-Lu fault zone: apatite fission-track and structural constraints from the Dabie Shan (eastern China). Tectonophysics 359:225–253

Groves DI, Goldfarb RJ, Gebre-Mariam M, Hagemann SG, Robert F (1998) Orogenic gold deposits: a proposed classification in the context of their crustal distribution and relationship to other gold deposit types. Ore Geol Rev 13:7–27

Gu HO, Xiao Y, Santosh M, Li WY, Yang X, Pack A, Hou Z (2013) Spatial and temporal distribution of Mesozoic adakitic rocks along the Tan-Lu fault, Eastern China: constraints on the initiation of lithospheric thinning. Lithos 177:352–365

Guan K, Luo ZK, Miao LC, Huang JZ (1998) SHRIMP zircon chronology for Guojialing suite granite in Jiaodong Zhaoye district. Sci Geol Sin 33:318–328, in Chinese with English abstract

Guo F, Fan WM, Wang YJ, Zhang M (2004) Origin of early cretaceous calc-alkaline lamprophyres from the Su–Lu orogen in eastern China: implications for enrichment processes beneath continental collisional belt. Lithos 78:291–305

Guo JH, Chen FK, Zhang XM (2005) Evolution of syn- to post-collisional magmatism from north Sulu UHP belt, eastern China: zircon U-Pb geochronology. Acta Petrol Sin 21:1281–1301, in Chinese with English abstract

Guo P, Santosh M, Li SR, Li Q (2014) Crustal evolution in the central part of eastern NCC: zircon U–Pb ages from multiple magmatic pulses in the Luxi area and implications for gold mineralization. Ore Geol Rev 60:126–145

Hamilton PJ, Kelley S, Fallick AE (1989) K-Ar dating of illite in hydrocarbon reservoirs. Clay Miner 24:215–231

Hou KJ, Li YH, Tian YR (2009) In situ U–Pb zircon dating using laser ablation multi ion counting-ICP-MS. Miner Deposita 28:481–492, in Chinese with English abstract

Hu SL, Wang SS, Shang HQ, Qiu J, Zhang RY (1987) Isotope ages of Linglong and Guojialing batholiths in Shandong Province and their geological implication. Acta Petrol Sin 3:83–89, in Chinese with English abstract

Hu FF, Fan HR, Yang JH, Wan YS, Liu DY, Zhai MG, Jin CW (2004) Mineralizing age of the Rushan lode gold deposit in the Jiaodong Peninsula: SHRIMP U-Pb dating on hydrothermal zircon. Chin Sci Bull 15:1629–1636, in Chinese with English abstract

Hu FF, Fan HR, Yang JH, Zhai MG, Xie LW, Yang YH (2007) Petrogenesis of Gongjia gabbro-diorite in the Kunyushan area, Jiaodong Peninsula: constraints from petro-geochemistry, zircon U–Pb dating and Hf isotopes. Acta Petrol Sin 23:369–380, in Chinese with English abstract

Huang ZC, Wang LS, Zhao DP, Mi N, Xu MJ (2011) Seismic anisotropy and mantle dynamics beneath China. Earth Planet Sci Lett 306:105–117

Huang C, Yu ZH, Zhang GL, Fu LT, Yuan ZY, Fan XY (2013) Cenozoic dextral strike-slip displacement of the middle Tan-Lu fault zone. J Jilin Univ (Earth Sci Ed) 43:820–832

Hurford AJ, Green PF (1983) The zeta age calibration of fission-track dating. Isot Geosci 1:285–317

Jackson SE, Pearson NJ, Griffin WL, Belousova EA (2004) The application of laser ablation-inductively coupled plasma-mass spectrometry to in situ U–Pb zircon geochronology. Chem Geol 211:47–69

Kerrich R, Goldfarb R, Groves D (2000) The characteristics, origins, and geodynamic settings of supergiant gold metallogenic provinces. Sci China Ser D Earth Sci 43:1–68

Ketcham RA, Donelick RA, Carlson WD (1999) Variability of apatite fission-track annealing kinetics: III. Extrapolation to geological time scales. Am Mineral 84:1235–1255

Koppers AAP, Morgan JP, Morgan JW, Staudigel H (2001) Testing the fixed hotspot hypothesis using 40Ar/39Ar age progressions along seamount trails. Earth Planet Sci Lett 185:237–252

Kuang YS, Pang CJ, Hong LB, Zhong YT, Xu YG (2012) Geochronology and geochemistry of the Late Cretaceous basalts in the Jiaolai Basin: constraints on lithospheric thinning and accretion beneath North China Craton. Geotecton Metallog 4:559–571, in Chinese with English abstract

Leech ML, Webb LE (2013) Is the HP–UHP Hong'an–Dabie–Sulu orogen a piercing point for offset on the Tan–Lu fault? J Asian Earth Sci 63:112–129

Li ZX (1994) Collision between the north and south China blocks: a crust-detachment model for suturing in the region east of the Tan-Lu fault. Geologija 22:739–742

Li ZL, Yang MZ (1993) The geology-geochemistry of gold deposits in Jiaodong region. Science and Technology Press, Tianjin, pp 1–42, in Chinese

Li HM, Mao JW, Shen YC, Liu TB, Zhang LC (2003a) Ar-Ar ages of K-feldspar and quartz from Dongji gold deposit, northwest Jiaodong, and their significance. Mineral Deposits 22:72–76, in Chinese with English abstract

Li JW, Vasconcelos PM, Zhang J, Zhou MF, Zhang XJ, Yang FH (2003b) 40Ar/39Ar constraints on a temporal link between gold mineralization, magmatism, and continental margin transtension in the Jiaodong gold province, Eastern China. J Geol 111:741–751

Li QL, Chen FK, Wang LX, Li XH (2006) Chemical procedure of ultra-low background and Rb–Sr dating of single mica. Chin Sci Bull 51: 321–325, in Chinese with English abstract

Li QL, Chen FK, Yang JH, Fan HR (2008) Single grain pyrite Rb–Sr dating of the Linglong gold deposit, eastern China. Ore Geol Rev 34:263–270

Li SR, Santosh M, Zhang HF, Shen JF, Dong GC, Wang JZ, Zhang JQ (2013) Inhomogeneous lithospheric thinning in the central North China Craton: zircon U–Pb and S–He–Ar isotopic record from magmatism and metallogeny in the Taihang Mountains. Gondwana Res 23:141–160

Li L, Santosh M, Li SR (2015) The 'Jiaodong type' gold deposits: characteristics, origin and prospecting. Ore Geol Rev 65:589–611

Ling WL, Xie XJ, Liu XM, Cheng JP (2006) Zircon U–Pb dating on the Mesozoic volcanic suite from the Qingshan Group stratotype section in eastern Shandong Province and its tectonic significance. Sci China Ser D Earth Sci 50:813–824

Liu S, Hu RZ, Zhao JH, Feng CX (2004) K–Ar geochronology of Mesozoic mafic dikes in Shandong Province, Eastern China: implications for crustal extension. Acta Geol Sin 78:1207–1213

Liu S, Hu R, Gao S, Feng C, Qi YQ, Wang T, Feng GY, CoulsoncIan M (2008) U–Pb zircon age, geochemical and Sr–Nd–Pb–Hf isotopic constraints on age and origin of alkaline intrusions and associated mafic dikes from Sulu orogenic belt, eastern China. Lithos 106:365–379

Liu S, Hu RZ, Gao S, Feng CX, Yu BB, Feng GY, Qi YQ, Wang T, Coulson IM (2009) Petrogenesis of Late Mesozoic mafic dykes in the Jiaodong Peninsula, eastern North China Craton and implications for the foundering of lower crust. Lithos 113:621–639

Liu S, Feng C, Hu R, Zhai M, Gao S, Lai S, Yan J, Coulson IM, Zou H (2014) Zircon U–Pb geochronological, geochemical, and Sr–Nd isotope data for Early Cretaceous mafic dykes in the Tancheng–Lujiang Fault area of the Shandong Province, China: constraints on the timing of magmatism and magma genesis. J Asian Earth Sci. doi:10.1016/j.jseaes. 2014.11.001

Luo WC, Wu QS (1987) Using altered minerals to determine mineralization ages of Jiaodong gold deposits. Chin Sci Bull 32:1245–1248, in Chinese with English abstract

Ma L, Jiang SY, Dai BZ, Jiang YH, Hou ML, Pu W, Xu B (2013) Multiple sources for the origin of Late Jurassic Linglong adakitic granite in the Shandong Peninsula, eastern China: zircon U–Pb geochronological, geochemical and Sr–Nd–Hf isotopic evidence. Lithos 162–163:251–263

Mercier JL, Hou MJ, Vergély P, Wang YM (2007) Structural and stratigraphical constraints on the kinematics history of the Southern Tan–Lu Fault Zone during the Mesozoic Anhui Province, China. Tectonophysics 439:33–66

Miao LC, Luo ZK, Huang JZ (1997) SHRIMP zircon study on the granitoid intrusion in the Zhaoye gold belt in Shangdong and its significance. Sci China Ser D Earth Sci 40:361–369 (in Chinese with English abstract)

Nasdala L, Hofmeister W, Norberg N, Martinson J, Corfu F, Dorr W, Sandra L, Kamo S, Kennedy A, Kronz A, Reiners P, Frei D, Kosler J, Wan Y, GTze J, HGer T, KrNer A, Valley J (2008) Zircon M257—a homogeneous natural reference material for the ion microprobe U–Pb analysis of zircon. Geostand Geoanal Res 32:247–265

Northrup CJ, Royden LH, Burchfiel BC (1995) Motion of the Pacific plate relative to Eurasia and its potential relation to Cenozoic extension along the eastern margin of Eurasia. Geology 23(8):719–722

Okay AI, Sengor AM (1992) Evidence for intracontinental thrust-related exhumation of the ultra-high-pressure rocks in China. Geology 20: 411–414

Qiu JS, Wang DZ, Luo QH, Liu H (2001a) ^{40}Ar-^{39}Ar dating for volcanic rocks of Qingshan Formation in Jiaolai basin, eastern Shandong Province: a case study of the Fenlingshan volcanic apparatus in Wulian County. Geol J China Univ 7:351–355, in Chinese with English abstract

Qiu JS, Xu XS, Luo QH (2001b) ^{40}Ar-^{39}Ar dating and source denoting of K-rich volcanic rocks and lamprophyres in western Shandong Province. Chin Sci Bull 46:1500–1508, in Chinese with English abstract

Qiu YM, Groves DI, McNaughton RJ, Phillips GN (2002) Nature, age, and tectonic setting of granitoid-hosted, orogenic gold deposits of the Jiaodong Peninsula, eastern North China Craton, China. Miner Deposita 37:283–305

Qiu JS, Liu L, Li YL (2012) Geochronology and geochemistry of potassic and sodic volcanic rocks in Tangtou basin, Shandong Province: implications for lithospheric thinning beneath the North China Craton. Acta Petrol Sin 4:1044–1056, in Chinese with English abstract

Ratschbacher L, Hacker BR, Calvert A, Webb LE, Grimmer JC, Mc Williams MD, Ireland T, Dong SW, Hu JM (2003) Tectonics of the Qinling (Central China): tectonostratigraphy, geochronology, and deformation history. Tectonophysics 366: 1–53

Ren FL, Zhang YQ, Qiu LG, Liu ZQ, Wang DH (2007) Evolution of the structural stress field in Jiaolai basin in Cretaceous. Geotecton Metallog 31:157–167, in Chinese with English abstract

Schmid JC, Ratschbacher L, Hacker BR, Gaitzch I, Dong SW (1999) How did the foreland react? Yangtze foreland fold-and-thrust belt deformation related to exhumation of the Dabie Shan ultrahigh-pressure continental crust (eastern China). Terra Nova 11(6):266–272

Sharp WD, Clague DA (2006) 50-Ma initiation of Hawaiian emperor bend records major change in Pacific plate motion. Science 313: 1281–1284

Slama J, Kosler J, Condon D, Crowley J, Gerdes A, Hanchar J, Horstwood M, Morris G, Nasdala L, Norberg N, Schaltegger U, Schoene B, Tubrett M, Whitehouse M (2008) Plesovice zircon—a new natural reference material for U–Pb and Hf isotopic microanalysis. Chem Geol 249:1–35

Song MC, Deng J, Yi PH, Yang LQ, Cui SX, Xu JX, Zhou ML, Huang TL, Song GZ, Song YX (2014) The kiloton class Jiaojia gold deposit in eastern Shandong Province and its genesis. Acta Geol Sin (Eng Ed) 88:801–824

Sun WD, Ding X, Hu YH, Li XH (2007) The golden transformation of the Cretaceous plate subduction in the west Pacific. Earth Planet Sci Lett 262:533–542

Tagami T, Shimada C (1996) Natural long-term annealing of the fission-track system around a granitic pluton. J Geophys Res 101:8245–8255

Tan J, Wei JH, Guo LL, Zhang KQ, Yao CL, Lu JP, Li HM (2008) LA-ICP-MS zircon U–Pb dating and phenocryst EPMA of dikes, Guocheng, Jiaodong Peninsula: implications for North China Craton lithosphere evolution. Sci China Ser D Earth Sci 51:1483–1500

Tang J, Zheng YF, Wu YB, Zha XP, Zhou JB (2004) Zircon U-Pb ages and oxygen isotopes of high-grade metamorphic rocks in the eastern part of the Shandong Peninsula. Acta Petrol Sin 20:1040–1061, in Chinese with English abstract

Tang J, Zheng YF, Wu YB, Gong B, Zha XP, Liu XM (2008) Zircon U–Pb age and geochemical constraints on the tectonic affinity of the Jiaodong terrane in the Sulu orogen, China. Precambrian Res 161: 389–418

Verdel C, van der Pluijm BA, Niemi N (2012) Variation of illite/muscovite ^{40}Ar-^{39}Ar age spectra during progressive low-grade metamorphism: an example from the US Cordillera. Contrib Mineral Petrol 164:521–536

Villa IM (1998) Isotopic closure. Terra Nova 10:42–47

Wan JL, Wang QL (1997) Fission track analysis on the active ages and thermal histories of Tancheng–Lujiang fault. Acta Geosci Sin 18: 73–76, in Chinese with English abstract

Wan TF, Zhu H (1996) The maximum sinistral strike-slip and its forming stage for the Tancheng–Lujiang fault zone. In: Zhao YH (ed) Formation and evolution of the Tancheng–Lujiang Fault Zone. China University Geosciences Press, Beijing, pp 56–69

Wang CM (2010) Metallogenic regularity and location prediction of the concealed gold deposits at depths. Postdoctoral dissertation, China University of Geosciences (Beijing), Beijing, p 377, in Chinese with English abstract

Wang LG, Qiu YM, McNaughton NJ, Groves DI, Luo ZK, Huang JZ (1998) Constraints on crustal evolution and gold metallogeny in the northwestern Jiaodong Peninsula, China, from SHRIMP U–Pb zircon studies of granitoids. Ore Geol Rev 13:275–291

Wang YS, Zhu G, Chen W, Song CZ, Liu GS (2005) Thermochronologic information from the Tan-Lu fault zone and its relationship with the exhumation of the Dabie Mountains. Geochimica 34:193–214, in Chinese with English abstract

Wang YS, Zhu G, Hu ZQ, Zhang BL, Xiang BW, Xie CL (2009) K-Ar dating of extensional fault gouge from the Yi-Shu segment of the Tan-Lu fault zone. Sci China Ser D Earth Sci 52:489–503

Wang CM, Zhang D, Wu GG, Xu YG, Carranza EJM, Zhang YY, Li HK, Geng JZ (2013) Zircon U-Pb geochronology and geochemistry of rhyolitic tuff, granite porphyry and syenogranite in the Lengshuikeng ore district, SE China: implications for a continental arc to intra-arc rift setting. J Earth Syst Sci 122: 809–830

Wang CM, Deng J, Carranza EJM, Santosh M (2014a) Tin metallogenesis associated with granitoids in the southwest Sanjiang Tethyan Domain: nature, types, and tectonic setting. Gondwana Res 26:576–593

Wang CM, Deng J, Santosh M, Lai XR (2014b) Nature, diversity and temporal-spatial distributions of sediment-hosted Pb-Zn deposits in China. Ore Geol Rev 56:327–351

Wang CM, Zhang D, Wu GG, Santosh M, Zhang J, Xu YG, Zhang YY (2014c) Geological and isotopic evidence for a magmatic-hydrothermal origin of the Ag-Pb-Zn deposits in the Lengshuikeng district, east-central China. Miner Deposita 49:733–749

Wang ZL, Yang LQ, Deng J, Santosh M, Zhang HF, Liu Y, Li RH, Huang T, Zheng XL, Zhao H (2014d) Gold-hosting high Ba-Sr granitoids in the Xincheng gold deposit, Jiaodong Peninsula, East China: petrogenesis and tectonic setting. J Asian Earth Sci 95:274–299

Wang CM, Deng J, Santosh M, Carranza EJM, Gong QJ, Xia R (2015) Timing, tectonic implications and genesis of gold mineralization in the Xincheng gold deposit, China: C-H-O isotopes, pyrite Rb-Sr and zircon fission track thermochronometry. Ore Geol Rev 65:659–673

Wilde SA, Zhou XH, Nemchin AA, Sun M (2003) Mesozoic crust–mantle interaction beneath the North China Craton: a consequence of the dispersal of Gondwanaland and accretion of Asia. Geology 31:817–820

Wu FY, Yang JH, Wilde SA, Zhang XO (2005) Geochronology, petrogenesis and tectonic implications of Jurassic granites in the Liaodong Peninsula, NE China. Chem Geol 221:127–156

Xie CL, Zhu G, Niu ML, Liu XM (2008) Geochemistry of Late Mesozoic volcanic rocks from the Chaohu-Lujiang segment of the Tan-Lu fault zone and lithospheric thinning processes. Acta Petrol Sin 24: 1823–1838, in Chinese with English abstract

Xu JW (1993) Historical review and present setting. In: Xu JW (ed) The Tancheng–Lujiang wrench fault system. Wiley, Chichester, pp 3–15

Xu JW, Zhu G (1994) Tectonic models of the Tan–Lu fault zone, eastern China. Int Geol Rev 36:771–784

Xu JW, Zhu G, Tong WX, Cui KR, Liu Q (1987) Formation and evolution of the Tancheng–Lujiang wrench fault system: a major shear system in the northwest Pacific Ocean. Tectonophysics 134:273–310

Xu JF, Sheng BR, Liu LZ, Zheng WS (1989) On the granitoids related to gold mineralization in Jiaobei block (in Chinese). J Geol Shandong Province 5:1–125, in Chinese with English abstract

Xu YG, Li HY, Pang CJ, He B (2009) On the timing and duration of the destruction of the North China Craton. Chin Sci Bull 54:3379–3396, in Chinese with English abstract

Yan JJ, Ma QG (1992) The Tancheng-Lujiang wrench fault system in the Bohai Bay area. Sci Geol Sin 17:31–38

Yang JH (2000) Age and metallogenic dynamics of gold mineralization in Jiaodong Peninsula, eastern China—constraints on the interaction of mantle/crust and metallogenesis/lithospheric evolution. PhD thesis, Institute of Geology and Geophysics, Chinese Academy of Sciences, p.133, in Chinese with English abstract

Yang JH, Zhou XH (2001) Rb–Sr, Sm–Nd, and Pb isotope systematics of pyrite: implications for the age and genesis of lode gold deposits. Geology 29:711–714

Yang JH, Wu FY, Wilde SA (2003) A review of the geodynamic setting of large-scale late Mesozoic gold mineralization in the North China Craton: an association with lithospheric thinning. Ore Geol Rev 23:123–152

Yang JH, Wu FY, Chung SL, Wilde SA, Chu MF, Lo CH, Song B (2005) Petrogenesis of Early Cretaceous intrusions in the Sulu ultrahigh-pressure orogenic belt, east China and their relationship to lithospheric thinning. Chem Geol 222:200–231

Yang KF, Fan HR, Santosh M, Hu FF, Wilde SA, Lan TG, Lu LN, Liu YS (2012) Reactivation of the Archean lower crust: implications for zircon geochronology, elemental and Sr–Nd–Hf isotopic geochemistry of late Mesozoic granitoids from northwestern Jiaodong Terrane, the North China Craton. Lithos 146–147:112–127

Yang LQ, Deng J, Goldfarb RJ, Zhang J, Gao BF, Wang ZL (2014) $^{40}Ar/^{39}Ar$ geochronological constraints on the formation of the Dayingezhuang gold deposit: new implications for timing and duration of hydrothermal activity in the Jiaodong gold province, China. Gondwana Res 25:1469–1483

Yin A, Nie S (1993) An indentation model for the North and South China collision and the development of the Tan-Lu and Honam fault systems, east Asia. Tectonics 12:801–813

Zhai MG, Santosh M (2013) Metallogeny of the North China Craton: link with secular changes in the evolving Earth. Gondwana Res 24:275–297

Zhai MG, Fan HR, Yang JH, Miao LC (2004) Large-scale cluster in east Shandong: anorogenic metallogenesis. Earth Sci Front 11:85–98

Zhai YS, Yao SZ, Cai KQ (2011) Economic geology, 3rd edn. Geological Publishing House, Beijing, pp 1–200, in Chinese

Zhang LC, Shen YC, Liu TB, Zeng QD, Li GM, Li HM (2002) Ar-Ar and Rb-Sr dating and metallogenic ages of gold deposits, Jiaolai Basin, Shandong Province. Sci China Ser D Earth Sci 39:727–734, in Chinese with English abstract

Zhang X, Cawood PA, Wilde SA, Liu R, Song H, Li W, Snee LW (2003a) Geology and timing of mineralization at the Cangshang gold deposit, north-western Jiaodong Peninsula, China. Miner Deposita 38: 141–153

Zhang YQ, Dong SW, Shi W (2003b) Cretaceous deformation history of the middle Tan-Lu fault zone in Shandong Province, eastern China. Tectonophysics 363:243–258

Zhang J, Zhao ZF, Zheng YF, Dai MN (2010) Postcollisional magmatism: geochemical constraints on the petrogenesis of Mesozoic granitoids in the Sulu orogen, China. Lithos 119:512–536

Zhang SH, Zhao Y, Davis GA, Ye Hao WF (2014) Temporal and spatial variations of Mesozoic magmatism and deformation in the North China Craton: implications for lithospheric thinning and decratonization. Earth Sci Rev 131:49–87

Zhao GT, Cao QC, Wang DZ, Li HM (1997) Zircon U-Pb dating on the Laoshan granitoids and its significance. J Ocean Univ Qingdao 27: 382–399, in Chinese with English abstract

Zhao GC, Sun M, Wilde SA, Li SZ (2005) Late Archean to Paleoproterozoic evolution of the North China Craton: key issues revisited. Precambrian Res 136:177–202

Zheng Y, Fu R, Xiong X (2006) Dynamic simulation of lithospheric evolution from the modern China and its surrounding areas. Chin J Geophys 49:415–427, in Chinese with English abstract

Zhou TH, Lu GX (2000) Tectonics, granitoids and Mesozoic gold deposits in East Shandong, China. Ore Geol Rev 16:71–90

Zhou TH, Goldfarb RJ, Phillips GN (2002) Tectonics and distribution of gold deposits in China—an overview. Miner Deposita 37:249–282

Zhou XH, Yang JH, Zhang LC (2003) Metallogenesis of superlarge gold deposits in Jiaodong region and deep processes of subcontinental lithosphere beneath North China Craton in Mesozoic. Sci China Ser D Earth Sci 46:14–25

Zhu G, Liu GS, Song CZ, Wang DX (2000) Pulsative extensional activity of the Tan–Lu Fault Zone. J China Univ Geosci 6(3):396–404, in Chinese with English abstract

Zhu G, Hou MJ, Wang YS, Liu GS, Niu ML (2004) Thermal evolution of the Tan–Lu Fault Zone on the eastern margin of the Dabie Shan and its tectonic implications. Acta Geol Sin Engl 78(4):940–953